HAL
open science

Seismic monitoring and modeling of an active volcano for prediction

Keiiti Aki, Valérie Ferrazzini

To cite this version:

Keiiti Aki, Valérie Ferrazzini. Seismic monitoring and modeling of an active volcano for prediction. Journal of Geophysical Research : Solid Earth, 2000, 105, pp.16,617-16,640. 10.1029/2000JB900033 . insu-03596935

HAL Id: insu-03596935

https://insu.hal.science/insu-03596935v1

Submitted on 4 Mar 2022

HAL is a multi-disciplinary open access archive for the deposit and dissemination of scientific research documents, whether they are published or not. The documents may come from teaching and research institutions in France or abroad, or from public or private research centers.

L'archive ouverte pluridisciplinaire **HAL**, est destinée au dépôt et à la diffusion de documents scientifiques de niveau recherche, publiés ou non, émanant des établissements d'enseignement et de recherche français ou étrangers, des laboratoires publics ou privés.

Copyright

JOURNAL OF GEOPHYSICAL RESEARCH, VOL. 105, NO. B7, PAGES 16,617–16,640, JULY 10, 2000

Seismic monitoring and modeling of an active volcano for prediction

Keiiti Aki[1]

Department of Earth Sciences, University of Southern California, Los Angeles

Valérie Ferrazzini

Observatoire Volcanologique du Piton de la Fournaise, Institut de Physique du Globe de Paris

Abstract. We describe seismic monitoring and modeling of an active volcano for the purpose of predicting the magma transport process in real time. We selected the Piton de la Fournaise, which has been monitored by an observatory since the early 1980s, and is active, with 28 eruptions from 1980 until August 1992. It erupted on March 9, 1998, after an unusually long quiet period. The eruption lasted until September 21, 1998. Before the March eruption, we completed the initial construction of a model of a magma system based primarily on long-period (LP) events and coda localization. We found that LP events are associated with the lateral movement of magma to the rift zone and not with the vertical movement to the summit. We also found that the source of 2 Hz LP events is located below that of 1 Hz LP events. The coda localization is a newly discovered phenomenon that helped to locate a magma body. This model was used for interpreting the incoming information from the precursory seismic crisis and the eruption tremor during the 6 months of the eruption. The simultaneous monitoring and modeling of an active volcano led us to a quantitative simulation of the eruption process, computing excess pressure and flow rate in a system of reservoirs connected by channels.

1. Introduction

The present paper describes seismic monitoring and modeling of the Piton de la Fournaise, an oceanic island volcano on La Réunion in the Indian Ocean, and lessons learned while trying to predict magmatic activity under the volcano.

Our main conclusion is that the construction of a physical model is essential for meaningful prediction in addition to observed precursory data. This obvious conclusion for any research in physical sciences is not easily achieved in the prediction research on natural hazards for several reasons. First, each case of the events to be predicted may be special both in time and space, and may not be repeatable. Testing of a model and drawing the interest and attention of a broad scientific community, needed for promoting the research, is then difficult. Since a prediction must be made using the knowledge available before the occurrence of the event, we are not allowed to go back and reconsider the event. Models we construct for interpreting monitoring observations must be able to cover a variety of possible scenarios. The science of prediction is an open-ended, evolving process, asking always "what's next?", and no definite answer may be obtained at any time. These difficulties are intrinsic to the prediction research, and must be dealt with if the scientific community accepts the prediction of natural hazards as an important goal.

It is our intention to show in the present paper that a sound science may be possible in prediction research coping with these difficulties. We shall describe the whole process of a prediction research inquiry, namely, the data analysis, the construction of a model, the testing of the model, and its updating. In section 2, we present the background information about the volcano, and describe, in section 3, the initial model primarily based on the data of long-period events since 1980. We then introduce in section 4, a new analysis of coda waves of volcano-tectonic earthquakes for tracing magma. The usefulness of coda waves for predicting a volcanic eruption was first recognized by *Fehler et al.* [1988] for Mount St. Helens, and convincingly demonstrated by *Londono et al.* [1998] for Nevado del Ruiz Volcano. The parameter coda Q, used in these studies, however, suffers from a large variability [*Aster et al.*, 1996]. We found that the spatial distribution of coda amplitude is more reliable and correlates well with the magmatic activity at Piton de la Fournaise. The model was revised based on the coda wave analysis, a few days before the eruption of March 9, 1998, which occurred after a 6 year period of repose. Section 5 describes how the model worked during the precursory seismic crisis of the eruption and how the model helped to interpret observations on the eruption tremors which lasted from March 9 to September 21, 1998. A further development of the model has resulted from its working with observations during the eruption, and an attempt is made for a quantitative simulation of the eruption process using a system of reservoirs and channels in section 6.

2. Background

Piton de la Fournaise (PdF), shown in Figure 1, is a basaltic island volcano like Kilauea, Hawaii. Both are intraplate

[1]Now at Observatoire Volcanologique du Piton de la Fournaise, Institut de Physique du Gloge de Paris, La Plaine des Cafres, La Réunion, France

Copyright 2000 by the American Geophysical Union.

Paper number 2000JB900033.
0148-0227/00/2000JB900033$09.00

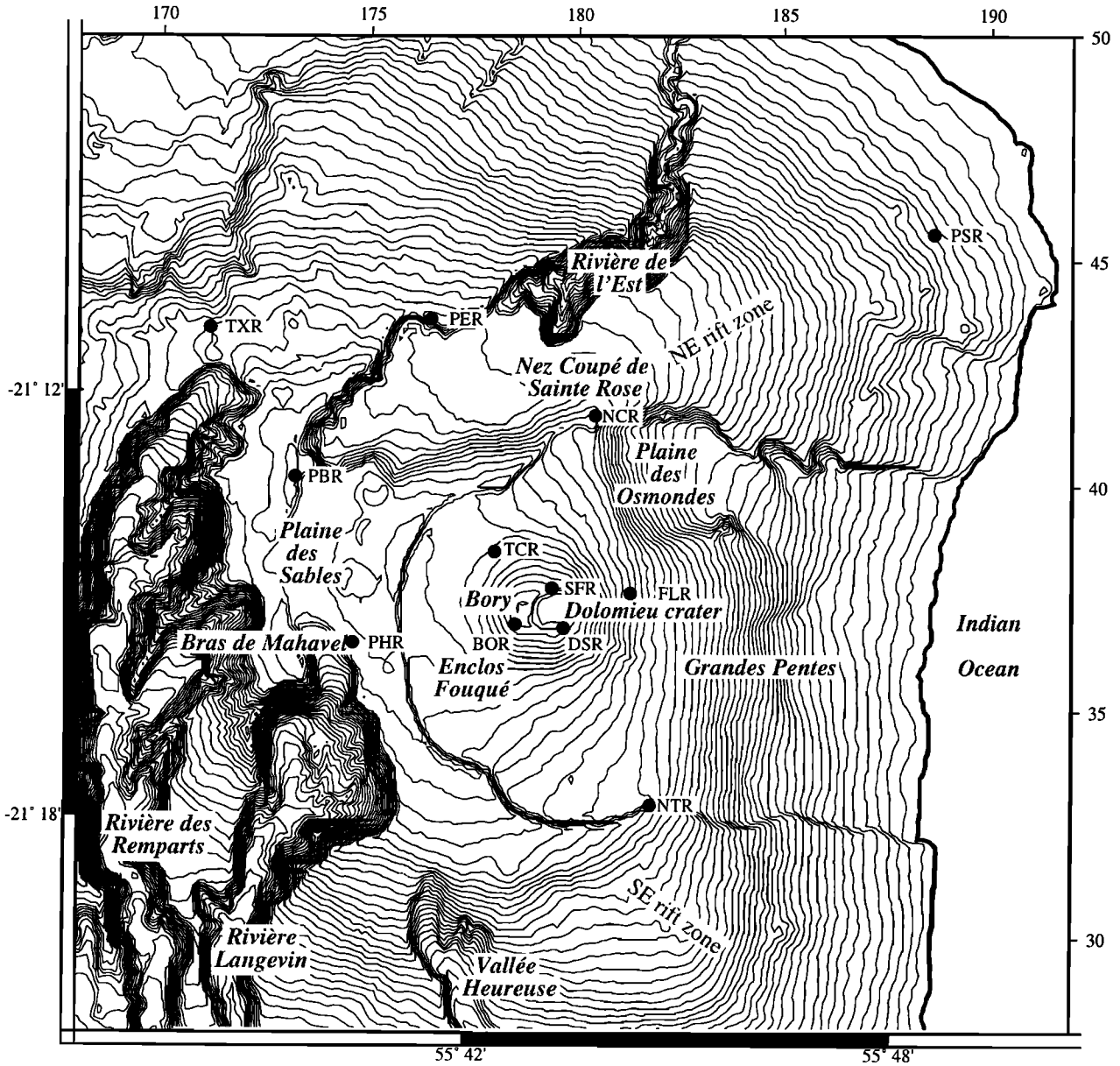

Figure 1. Topography map of the PdF, showing craters Bory and Dolomieu at the summit of the central cone, the Enclos (Fouque) caldera, and the northeast and southeast rift zones. The locations of seismic stations within the map area are also marked. Stations outside the map area are shown in Figure 11. The numbers on the top and right sides of the map indicate respectively the eastward and northward coordinates in kilometers with the origin at (21.5°S, 54.0°E).

volcanoes on an oceanic lithosphere, with a supply of magma from hot spots in the mantle. The rate of erupted magma is not much different between the two volcanoes. An estimate for Kilauea by *Dzurisin et al.* [1984] for the period from 1956 to 1983 is 30 million m^3yr^{-1}, while *Lénat and Bachèlery* [1988] gave 10 million m^3yr^{-1} for the PdF during the period from 1930 to 1985. Since *Dzurisin et al.* [1984] estimated that 65% of the magma supplied from the upper mantle remains in the rift zone under Kilauea, while there is no evidence for such a steady accumulation of magma in the rift zone of Piton de la Fournaise, the difference in magma supply from the upper mantle may be about a factor of 10 between the two volcanoes. The rift zone clearly exists in PdF, as demonstrated by eruptions along the northeast rift zone outside the Enclos caldera in April 1977 and a series of fissure eruptions extending from the summit to the south coast in March 1986. It is also clear that the rift zone is not developed here as well as in the Hawaiian volcanoes. From a sea beam bathymetry survey, *Lénat et al.* [1989a] found that the active rift zones of PdF widen downslope unlike typical Hawaiian rift zones, which form narrow ridges extending tens of kilometers offshore.

Nakamura [1980] was the first to ask why long rift zones develop in Hawaiian volcanoes. Comparing with the Galapagos Islands, another intraplate basaltic volcano lacking a rift zone and located on a young lithosphere, he suggested that the rift zone intrusion in Hawaii is sustained by repeated Kalapana-type earthquakes caused by a slip along the top of the oceanic crust which may have anomalously low friction due to a thick

sediment and a high pore pressure [*Hubbert and Rubey*, 1959]. This idea has been supported by more recent works [e.g., *Dieterich*, 1988; *Thurber and Gripp*, 1988].

PdF is located on an old oceanic lithosphere with a flexural rigidity [*Walcott*, 1970; *Bonneville et al.*, 1988] comparable to the Hawaiian lithosphere, and the oceanic crust upon which the volcano was built must have had a thick sediment cover. There is, however, a major difference in the speed of lithosphere relative to the mantle under these two volcanoes. In Hawaii, the old oceanic crust is always present in front of the youngest volcano due to the high plate speed, and the Kalapana-type earthquake occurs along the weak plane formed by the deep sea sediment, sustaining the intrusion into the rift zone. On the other hand, the African plate, on which PdF is located, moves so slowly that a fluctuation in the path of magma ascent in the crust can move the volcano back and forth, allowing the remains of proto Fournaise volcano, as evidenced from the old magma chamber encountered by deep drilling [*Rancon et al.*, 1989] as well as the gravity highs deviating from the current summit area [*Rousset et al.*, 1989], to prevent the full development of a rift zone. Thus it is more difficult for magma to intrude into the rift zone here than in Hawaii, and that explains why PdF has a remarkable central cone as high as 500 m from the floor of the Enclos caldera due to repeated summit eruptions, which is absent in the Kilauea volcano.

3. Magma System Defined by the Use of Long-Period Events

Active volcanoes generate the so-called " long-period (LP] events" (see, for example, *Chouet* [1996] for a review] in addition to usual earthquakes indistinguishable from those of tectonic origin found elsewhere. They are distinguished from the latter by an emergent onset, a lack of clear ***S*** phase, and a lack of the high-frequency part of the spectrum expected for a tectonic earthquake of a similar size. Key questions about LP events are whether their seismic sources involve magma and if so, how. From 1981 to 1992, PdF had 28 eruptions and we were able to identify about 800 LP events during this period.

3.1. Identification of Long-Period Events

Seismological investigations on eruptions at PdF since the establishment of the observatory were described in journal papers by individual scientists [*Bachèlery et al.*, 1982; *Lépine*, 1987; *Lénat et al.*, 1989b, c; *Delorme et al.*, 1989; *Hirn et al.*, 1991; *Grasso and Bachèlery*, 1995; *Nercessian et al.*, 1996; *Sapin et al.*, 1996] as well as in the annual report of the world volcanic eruptions in *Bulletin of Volcanology*. It was found that almost all the eruptions were preceded by a "seismic crisis" which is a swarm of volcano-tectonic earthquakes occurring beneath the central cone. The seismic signature of the eruption itself is characterized by steady continuous tremors originating from the eruption site. In addition to the above swarm of shallow volcano-tectonic events and the eruption tremors, there have been occasional mention of "low-frequency events", but they have not received much attention partly because their occurrences are not simply related to eruptions, and partly because of the difficulty in discriminating them from other seismic events such as numerous rockfalls along the steep valleys of the island and ***P***, ***S*** and ***T*** phases from earthquakes along active mid-ocean ridges in the Indian Ocean.

We developed a reliable method for discriminating a long-period event originating from the volcano from events coming from elsewhere. Since we cannot apply the classical method for locating tectonic earthquakes to them because of the lack of clear onset for ***P*** and ***S*** waves, we relied on their spatial distribution of amplitude across the network. For this purpose it is essential to eliminate the local effect of the recording site from the observed amplitude. *Koyanagi et al.* [1995] have demonstrated that the coda amplification factor applicable to ***S*** waves [e.g., *Kato et al.*, 1995; *Sato and Fehler*, 1998] can be effectively used to smooth the amplitude distribution of ***T*** phase recorded by the seismic network of Hawaii. The apparent dominance of ***S*** waves in seismic waves converted from the acoustic waves in the oceanic waveguide may be understood from the order of magnitude greater conversion coefficient from ***P*** to ***S*** as compared to that from ***S*** to ***P*** by localized heterogeneities [*Aki*, 1992; *Zeng*, 1993].

In order to obtain the station amplification factor by the coda method, we used a volcano-tectonic event with a high signal-to-noise ratio at a lapse time (time measured from the origin time of the event) sufficiently larger than the arrival time of the primary and forward scattered waves. The choice of lapse time twice the ***S*** wave arrival time, originally adopted for central Asia by *Rautian and Khalturin* [1978], has been found adequate for most parts of the world. We found, however, that at La Réunion, the station site factor depends on the distance from the event location to the summit area. To avoid this effect, we used an event distant from the volcano, a ***M***=3 event (the largest we have seen so far originating from in and near La Réunion) located offshore near the northern end of the island. The dominant frequency of analyzed coda of this event was 2 to 3 Hz at all stations.

We tested the coda amplification factor using seismic data from a known source, rockfalls in the Bras de Mahavel

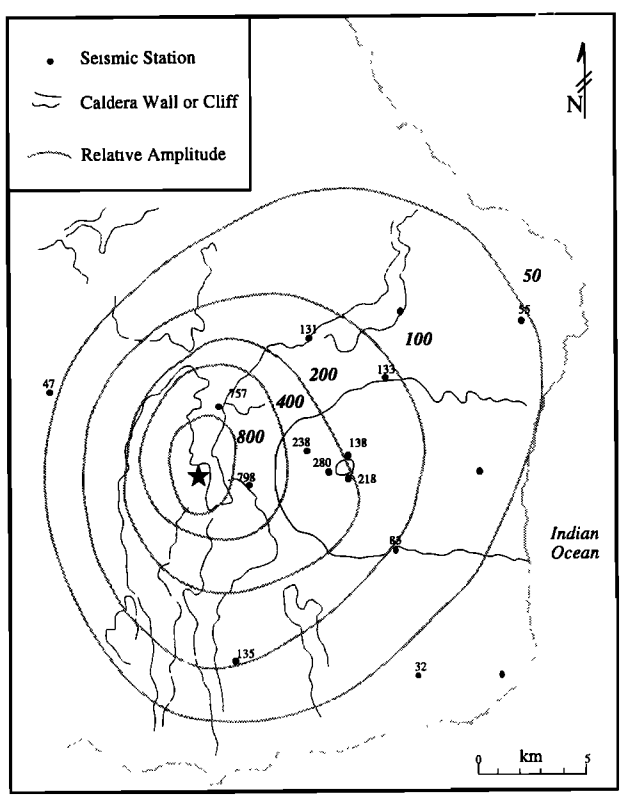

Figure 2. Amplitude distribution of seismic waves in the frequency band from 1 to 3 Hz from a Mahavel rockfall. See Figure 1 for latitude and longitude.

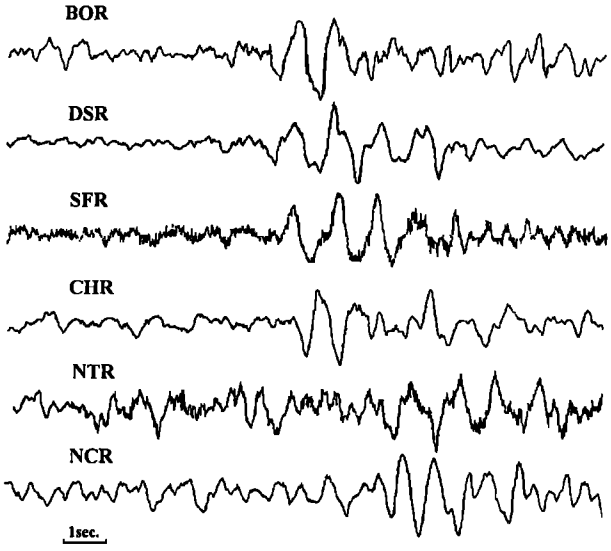

Figure 3. Seismograms of one of the simplest LP events with relatively short duration and long period.

occurring in June-July 1995. Owing to steep cliffs and deep valleys (see Figure 1), rockfalls are very common sources of seismic signals on this island. The depth of the valley of Bras de Mahavel is about 800 m. Figure 2 shows the maximum amplitude of one of the largest Mahavel rockfall events in micrometers per second reduced to the common site conditions at station BOR using the coda site factor. The dominant frequency was around 3 Hz at all stations. The variation of the amplitude corrected for the station site effect is smooth enough for drawing isoamplitude contours at intervals of a factor of 2. The center of contours agrees well with the site of the rockfall, and the stronger decrease in amplitude toward the west than the east is expected because the rockfalls occur on the eastern slope of the valley. The decrease of amplitude with distance toward the east can be fitted with the formula for surface waves with the attenuation specified by a Q factor of 40 to 60. This range of Q agrees well with the value obtained by *Koyanagi et al.* [1995] for the summit area and rift zones of Kilauea, from the amplitude decay of T phases. We also tested the site factor using T phases with satisfactory results, showing amplitude decreasing smoothly from the coast to inland.

To study the amplitude distribution for LP events, we first analyzed a seismic crisis in December 1991. This crisis is called an intrusion event, because there was no eruption of magma although both seismic and geodetic observations showed activities similar to those preceding eruptions. The seismic crisis started with a swarm of shallow volcano-tectonic earthquakes with dominant frequencies higher than 10 Hz beneath the summit at about 0505 UT on December 7, 1991. After a vigorous occurrence of these events for about 20 min, low-frequency motions appeared, forming the background over which high-frequency events are superposed. This low-frequency background reached a peak at 0541. As the seismic activity declined, discrete LP events began to appear at about 0556. The low-frequency background and LP events must come from a common source since their amplitude distributions across the network were identical. Figure 3 shows records of one of the simplest LP events with the shortest duration and longest period. The three summit stations, BOR, SFR, and DSR located near the rim of the summit craters called Bory and Dolomieu (Figure 1) at an elevation of 2500 m above sea level, have very similar waveforms. Their arrival times and amplitudes after correction for the site effect are also very similar. This excludes the possibility that they may be due to rockfalls near the summit, since the latter generate waves of much higher frequency which vary among the summit stations in the arrival time, amplitude, and frequency content.

For their discrimination from rockfalls outside the summit area and events outside the island, we study the amplitude distribution of LP events. We selected 11 events from the December 1991 crisis with a dominant frequency ranging from 1.0 to 3.3 Hz. We extended the list by searching for events of similar nature both before and after the crisis, and determined the amplitude distribution for 31 events as listed in Table 1, which gives the date and time of the event, the maximum amplitude at BOR measured on the Sefram paper record in millimeters (at a nominal sensitivity of 0.34 $\mu ms^{-1}mm^{-1}$), dominant frequency in hertz, and duration in seconds. The table also gives the maximum amplitude at each station divided by the mean of the maximum amplitudes at the three summit stations. In general, LP events show the largest amplitude at the summit and are rarely observed at stations more than 10 km away from the summit. We did not recognize any obvious difference in amplitude distribution among events with different dominant frequencies.

The events listed in Table 1 were divided into three periods, before, during, and after the December 1991 crisis, and we plotted the median value of normalized amplitude for each station in Figures 4a, 4b, and 4c, respectively. The isoamplitude contours for 0.5 and 0.25 are also shown in these figures. Comparing them with the similar contours for the Mahavel rockfall shown in Figure 2, the spacing between the contour map for LP events is broader at shorter distance than in the case of the rockfall, implying that the sources of LP events are located at some depth beneath the summit, and are composed of body waves. This conclusion is consistent with the observed similarity in arrival time, amplitude, and waveform at the three summit stations.

In order to estimate the depths of LP events, we compared them with the volcano-tectonic events of the December 1991 crisis, which are located just above sea level. We filtered records of one of the largest volcano-tectonic events occurring at 0514, December 7, 1991, through a passband between 1 and 3 Hz and plotted the amplitude relative to BOR in Figure 4d in the same way as shown in Figures 4a, 4b, and 4c. The amplitude contours for the band-pass-filtered volcano-tectonic event are similar to those for LP events, indicating that locations of the sources of LP events are close to the hypocenters of the cluster of the volcano-tectonic event.

Certain stations show anomalously high values of normalized amplitude, for example, station LCR in Figure 4a, station PHR in Figure 4c, and station PSR in Figure 4d. These signals might be enhanced in a particular direction due to some waveguide effect of magma path. We observed a similar effect on the amplitude distribution of long-period tremor immediately preceding the eruption of March 9, 1998 (Figure 20), and later when the eruption occurred outside the Enclos caldera (Figure 25a).

Although most of the LP events recorded by the network until 1995 occurred beneath the summit at about sea level, there were a few different sources of LP events. One of them was characterized by high dominant frequencies in the range from 4 to 9 Hz and occurred from March 26 to April 5, 1986, during a pit crater collapse in the summit caldera following eruptions in the southeast rift zone [*Lépine*, 1987; *Hirn et al.*, 1991]. The other is a swarm of LP events characterized by a single

Table 1. Table of Normalized Amplitude for Larger LP Events

Date	time	Amplitude mm	Frequency Hz	Duration sec	CHR	PER	NCR	NTR	PHR	PBR	LCR
Nov 26, 1990	20:47	100	1.7	60	...	0.43	0.36	...	...	0.36	0.36
Dec. 11, 1990	10:08	50	1.7	20	...	0.52	0.52	0.67	...	0.88	. .
March 2, 1991	11:52	30	1.4	18	0.80	0.30	0.52	0.83	.	0.58	..
March 10, 1991	09:40	20	1.7	40	0.71	0.32	0.40	0.53	.	0.39	0.58
March 12, 1991	23:34	20	1.4	40	0.56	0.27	0.40	0.52	..	0.35	
March 15, 1991	20:14	20	1.8	22	0.68	0.35	0.44	0.49	.	0.43	1.13
March 16, 1991	22:44	25	1.5	20	0.74	...	0.45	0.42	...	0.35	0.95
March 17, 1991	20:36	20	1.3	11	0.79	0.32	0.38	0.38	...	0.30	1 11
March 18, 1991	08:20	70	1.5	30	0.54	0.23	0.33	0.32	.	0.29	
March 25, 1991	23:52	45	1.4	50	0.73	..	0.46	0.45	..	0.36	
March 27, 1991	16:10	60	1.4	35	0.94	..	0 55	0 56	..	0 52	1.36
March 29, 1991	03:18	50	1.4	35	0.61	..	0.56	0.81	.	0.54	
April 8, 1991	13 48	40	1.4	28	0.53	. .	0.51	0.35	.	.	0 56
April 8, 1991	19:43	40	1.5	16	0.76	. .	0.60	0 90	.	..	.
Dec. 7, 1991	12:05	15	2.8	23	0.61	0.17	0.43	0 40	0.38	..	0.11
Dec. 7, 1991	12:17	25	3.3	30	0.53	...	0.58	...	0.83	0.36	.
Dec. 8, 1991	23:42	20	2.2	11	...	0.36	0.40	0.36	0.55	0.17	. .
Dec. 9, 1991	03:06	45	1.4	18	0.50	0.43	0.38	0.60	0.44	0.32	0.49
Dec. 9, 1991	11:15	45	1.4	18	0.51	0.45	0.19	0.55	0.42	0.26	0.39
Dec. 9, 1991	04:57	15	2.2	20	0.64	0.27	0.32	0.60	...	...	0.21
Dec. 10, 1991	21:14	20	1.0	15	0.65	...	0.42	0.29	0 40	0.25	...
Dec. 10, 1991	21:15	30	1.0	25	0.66	0.39	0.54	0.51	...	0.35	0.32
Dec. 11, 1991	13:07	20	1.0	15	0.57	...	0.57	0.53	0.63	0.47	0.42
Dec. 11, 1991	16:45	15	1.0	12	0.71	...	0.36	0.48	0.36	0.38	0.35
Dec. 11, 1991	16:46	15	1.0	12	0.52	...	0.24	0.54	0.41	...	...
Dec. 16, 1993	11 :17	60	2.0	50	0.75	0.75	0.35	0.58	0.69	0 40	...
Jan. 18, 1994	10:10	25	2.0	18	0.80	0.58	0.44	0.51	...	0.35	..
Oct 30, 1994	17:50	60	2.4	30	0.50	0.28	0.44	0.56	0.64	0.28	0.40
Oct. 30, 1994	17:53	22	2.0	15	0.81	0.53	0.44	0.71	0.76	0.51	0.74
Dec. 27, 1994	16:44	50	2.6	37	0.75	0.39	0.45	0.43	0.79	0.47	0.36
April 1, 1995	04:24	50	2.6	18	0.68	...	0.47	0.42	0.63	0.37	0.26

frequency of 3.5 Hz recorded only at station NCR throughout 1987, but mostly from June to September. The narrow spectrum and strong attenuation suggest that they may be trapped vibrations in a low velocity body, such as a pocket of magma. On the other hand, unlike rift zones in Hawaii, there is no clear geological evidence for magma pocket under the rift zone of PdF.

LP events and tremors occur at various depths down to about 50 km under Kilauea, Hawaii [*Koyanagi et al.*, 1987]. Deep LP events are more difficult to identify than the shallow ones, because of their similarity with ***P*** and ***S*** waves from distant events outside the island. We expect that a deep LP event will show a similar amplitude and spectral shape at all stations as for records of most events originating from outside the island. In an intensive search for a deep LP event in the past, all the candidates selected turned out to be from somewhere outside La Réunion: many earthquakes in the mid-ocean ridges of the Indian Ocean, two earthquakes in the Mascarene plateau, one in Madagascar, and an offshore slow earthquake near La Réunion.

3.2. History of LP Events Since 1985

In order to study the occurrence of the LP events in relation to the eruption history of the volcano, we measured the time of occurrence of the event, the maximum amplitude at station BOR, the duration of the event, and its dominant frequency. The identification of LP events is primarily based on the Sefram paper records at eight selected stations. The criteria for the identification of LP events are (1) the dominant frequency is less than about 3 Hz, (2) there is coherency of waveform at the three summit stations, and (3) the amplitude is maximum in the summit area, and negligible at stations farther than 10 km from the summit. The Sefram record includes necessary information for the above criteria, except for small events to which criterion 3 is difficult to apply due to noise at stations far away from the summit and closer to the ocean.

The Sefram records for selected periods and events since the beginning of the observatory in early 1980s are archived. The selection depends on the personnel in charge, and might have not been uniform in time. Our current list of LP events starts with the seismic crisis of August 5, 1985. The characteristics of 13 LP events during this crisis are very similar to those of the December 1991 crisis described in the preceding section. The list includes about 800 LP events from August 1985 to the present. It may be not complete. We might have missed some LP events that were not kept. On the other hand, some of the listed LP events with small amplitude may be outside events. For example, our list includes about 150 LP events in the 4-year period from 1985 through 1988, while it contains about 650 in the same 4-year period from 1989 through 1992. Considering the higher rate of eruptions in the earlier period than the later, it is possible that some LP events in the earlier period might have been lost. On the other hand, about 120 events listed for the latest 4-year period 1993 through 1996 may contain a relatively greater number of outside events that are misidentified as LP events because we looked hard for possible LP events in the easily accessible more recent data. Thus in spite of the possible nonuniformity in the data selection, we may conclude that the rate of occurrence of LP events was many times lower in the last 4-year period during which there was no eruption, as compared to the preceding 8-year period, in which more than 20 eruptions occurred.

Among the parameters in the list, the dominant frequency is less dependent than the other parameters on a possible temporal change in the instrument characteristics such as gain setting. We measure the dominant frequency of an LP event by counting the number of peaks of the wave train of 5 s duration in which the maximum amplitude of the event occurs. The shape of the

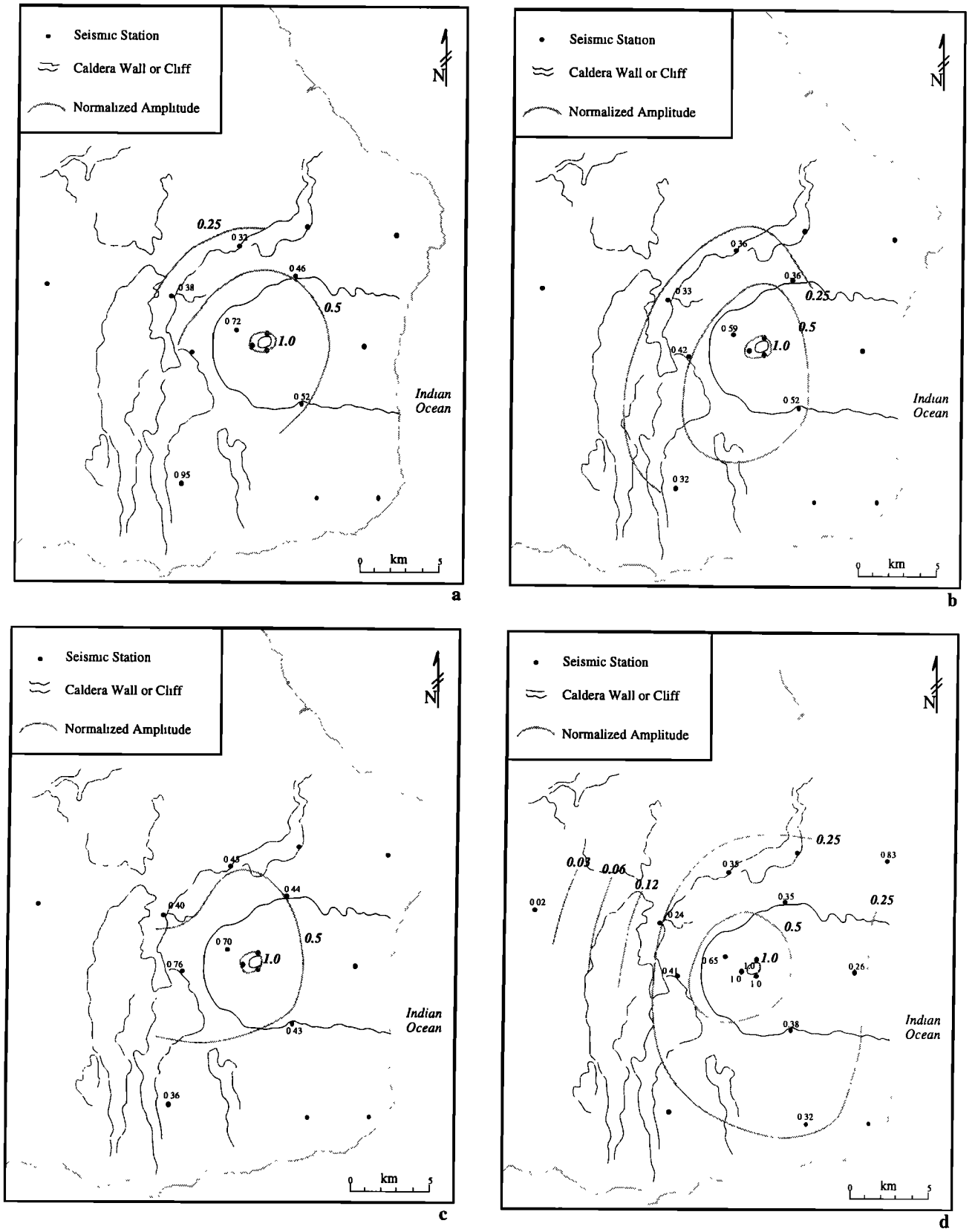

Figure 4. Distribution of median amplitude of LP events normalized to the mean of the three summit stations, obtained from (a) 14 events occurred in the period from 1990 to April 1991, (b) 11 events during the intrusion crisis of December 1991, and (c) six events after the crisis till April 1995. Figure 4d shows the distribution of amplitude of a large volcano-tectonic event during the crisis of December 1991, band-pass filtered between 1 and 3 Hz. The number attached to each station is normalized to the mean of the three summit stations. See Figure 1 for latitude and longitude.

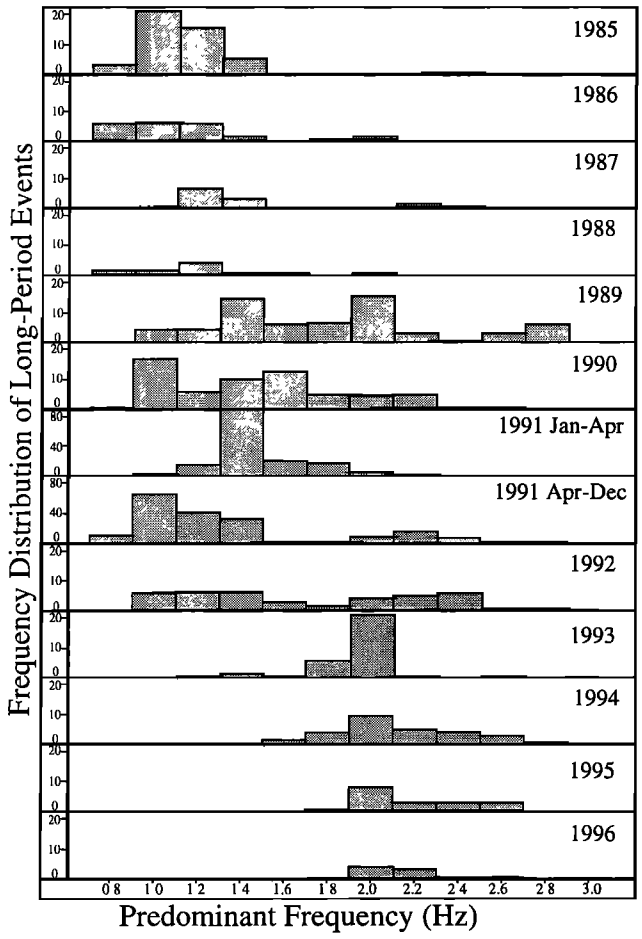

Figure 5. The histogram of annual occurrence of LP events with a given dominant frequency. The vertical scale is common to all years, except for 1991, for which it is 4 times greater than the rest, even though the year is separated into two parts.

frequency distribution of the occurrence of the dominant frequency may be least affected by the judgment used for selecting records.

Figure 5 shows a histogram of the number of occurrences of LP events with a given dominant frequency for each year from 1985 through 1996. (The data are given in Table 2.) The scale of the vertical coordinate in Figure 5 is common to the entire period except for 1991, in which two distinct swarms of LP events occurred in two separate periods, January through April and December, and histograms are shown separately for the two periods (there were no LP events from May to November 1991). In order to find any trend in Figure 5 related to the eruption history, we show the amount of magma erupted in each eruption since 1985, as described in the annual report of the world volcanic eruption in *Bulletin of Volcanology*, in Figure 6, for three different eruption types: summit, rift zone, and intermediate zone.

The most outstanding trend in the distribution of the dominant frequency is the systematic disappearance of LP events after the last eruption of August 1992. LP events with the lowest frequency disappeared first. No events with a dominant frequency of 1 Hz occurred since 1993 until 5 hours before the March 1998 eruption. Those with dominant frequencies around 2 Hz become dominant in 1993, decreased gradually, and practically vanished in 1996. A 2 Hz LP event located beneath the summit reappeared on June 4, 1997.

During the same period the activity of the volcano-tectonic earthquakes also declined gradually, as shown in Figure 7. The rate of their occurrence, however, did not become zero. The rate for 1995 is about one half of that for 1993, and furthermore there has been an indication of revival in 1996. The above difference between the volcano-tectonic earthquake and the LP event can be explained if the former is due to stress transfer without direct magma involvement, but the latter requires the presence of magma in the source region. The path of magma under PdF is characterized by a high-velocity body according to the refraction, wide-angle reflection, and tomographic studies by *Nercessian et al.*, [1996] and *Driad* [1997], and the high-velocity body may act as a stress guide and cause a stress concentration at the junction of the summit path and the rift zone path, resulting in a swarm of volcano-tectonic events there whenever magma moves rapidly somewhere.

The observed disappearance of 1 Hz LP events preceding that of 2 Hz LP events during the above period of declining volcanic activity suggests that the 1 Hz source may be located above the 2 Hz source because it lost magma first. This picture of shrinking reservoir is consistent with the result of a Global Positioning System (GPS) survey by *Briole et al.* [1998], who found that the summit area showed a slow contraction from 1992 to 1996.

We may summarize the above inference into the first element of our model that the source of 1 Hz LP events is separated from that of 2 Hz LP events and located above the latter.

The trend of increasing lower limit of the dominant frequency can be seen in Figure 5 also from 1985-1986 to 1988-1989, corresponding to a period of eruptive activity ending in 1989, in which two dominant peaks coexist at 1.4 and 2 Hz. There was no eruption in 1989, but we find two eruptions in 1990, in

Table 2. The Annual Number of LP Events With a Given Range of Predominant Frequency

Year	0.8-0.9	1.0-1.1	1.2-1.3	1.4-1.5	1.6-1.7	1.8-1.9	2.0-2.1	2.2-2.3	2.4-2.5	2.6-2.7	2.8-2.9
1985	3	21	15	5	0	0	0	0	1	0	0
1986	6	7	6	2	0	1	2	0	0	0	0
1987	0	1	7	3	0	0	0	2	1	0	0
1988	2	2	4	1	1	0	1	0	0	0	0
1989	0	4	4	14	6	7	15	3	1	3	6
1990	1	17	6	10	13	5	4	5	1	1	0
1991a	0	3	17	93	21	18	6	2	0	0	0
1991b	12	68	44	34	4	3	8	16	7	3	4
1992	0	6	7	7	3	2	4	5	6	1	1
1993	0	0	1	2	1	6	21	1	0	1	0
1994	0	0	0	1	2	4	9	5	4	3	1
1995	0	0	0	0	0	1	8	3	3	3	0
1996	0	0	0	0	0	0	4	3	1	1	0

Range of predominant frequency is in hertz. The period January 1 to April 30, 1991 is denoted as 1991a; The period December 1 to December 31, 1991 is denoted as 1991b.

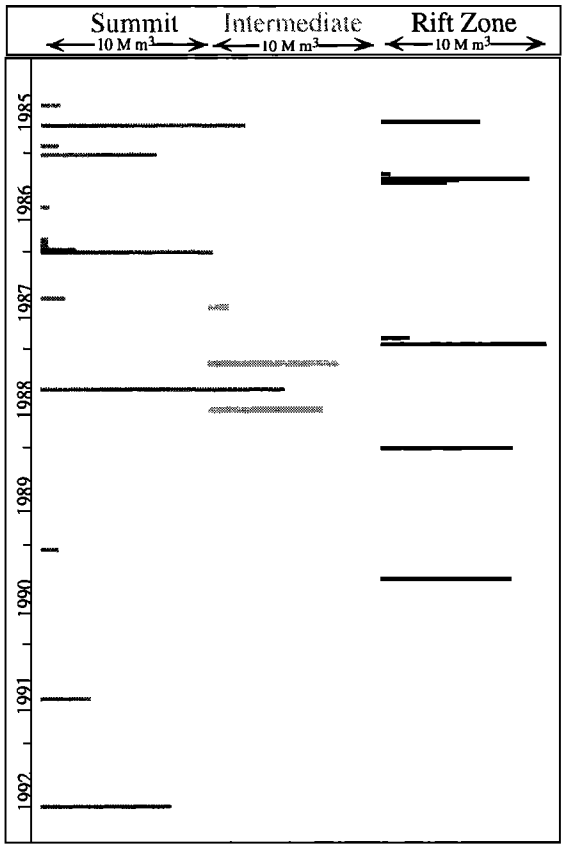

Figure 6. Amount of erupted magma for the three types of eruptions classified according to the elevation of the eruption site from 1985 to 1992.

which the 1 Hz source became active again. Whether the 1.4 Hz source is a shrunken state of the 1 Hz source or a separate system is an open question. However, the swarm of LP events during January-April 1991, which is clearly dominated by this source (Figure 5), is the only major LP swarm that has no direct relation to any particular eruption or intrusion event, and this swarm apparently ended with a strong shaking by a M=5.8 earthquake in Madagascar 800 km away from La Réunion. These observations suggest that the source of 1.4 Hz LP events corresponds to a low-energy state of the magma system, and we prefer the idea that this source of LP events is not independent, but corresponds to a shrunken state of the 1 Hz LP source.

3.3. Relation of LP Events to Individual Eruptions

A cursory look at the eruption history and the occurrence of LP events leads to some disappointment from the viewpoint of prediction because they seem to occur more often following an eruption rather than preceding one. Table 3 lists 17 seismic crises observed by the observatory network since 1985. The table is not complete because the Sefram record for the period preceding some of the eruptions in 1985 through 1987 could not be found so far. Nevertheless, this table can be summarized as follows:

1. The 17 crises start with a swarm of volcano-tectonic events located beneath the central cone at about sea level, with only one exception, crisis 2, in which they are located on the east side of the central cone at deeper depths. Crisis 2 was not followed by an eruption.

2. Of the remaining 16 crises, three crises including the recent one on November 26, 1996, were not followed by an eruption.

3. For the 13 crises preceding an eruption, the precursory time between the onset of the crisis and the beginning of the eruption, estimated from the records of eruption, ranges from 17 min to 9 hours 24 min. As shown in Figure 8, the precursory time is less than 1 hour for eruptions near the summit and more than 6 hours for eruption sites with an elevation lower than 1800 m. *Bachèlery et al.* [1998] recognized a similar correlation between the duration of geodetic disturbance associated with a seismic crisis and the distance of the eruption site from the summit, which increases with decreasing elevation.

4. The majority of seismic crises start with a swarm of volcano-tectonic earthquakes located beneath the central cone and end with continuous tremor from the eruption site. Four eruptions (crises 3, 5, 11, and 13) near the rim of the Enclos caldera, were preceded by a swarm of LP events which we now associate with the magma reservoir beneath the central cone. LP events are completely missing in the precursory crises of all other eruptions in the list.

The above observations suggest two distinct paths of magma to the eruption site under PdF, the summit path and the rift zone path. An eruption through the summit path starts at elevations higher than about 2100 m on fissures that extend downward. The precursory seismic swarm lasts for less than about 2 hours and does not include LP events. The LP events may occur, however, during or immediately after the summit path eruption as in September 1985, December 1985, February 1987, and September 1992. On the other hand, an eruption through the rift zone path occurs at elevations lower than about 2100 m on fissures which sometimes extend upward as in December 1988. The precursor seismic swarm lasts longer than about 2 hours and includes LP events. Thus the LP source is located on the rift zone path and not on the summit path. The reason why some summit eruptions accompany LP events at its later stage may be the diversion of magma flow from the summit path to the rift zone path. In some cases, such a diversion may stop a summit eruption.

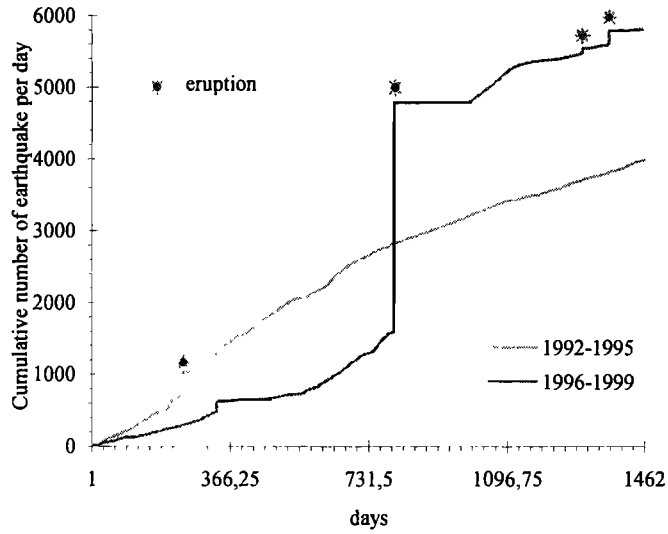

Figure 7. Annual cumulative number of volcano-tectonic events under the Piton de la Fournaise for 1992 through 1996. The step-like change in 1992 is the seismic crisis precursor to the last eruption before the March 1998 eruption, and the one in 1996 is the crisis of November 26 referred to as Crisis 1 in sections 4 and 5 of this paper.

Table 3 Seismic Crises at the Piton de la Fournaise

Crisis	Date	Precursory Time	Elevation of the Eruption Site
1	June 14, 1985	less than 1 hour	2500 m
2	July 10, 1985		no eruption
3	Aug. 5, 1985	2 hour 37 min.	2100-2000 m
4	Dec. 1, 1985	17 min.	2500-2100 m
5	March 18, 1986	9 hour 24 min.	1750-1720 m
6	June 2, 1987		no eruption
7	July 19, 1987	2 hour 13 min.	2050-2000 m
8	Fev. 7, 1988	2 hour 5 min.	2000 m
9	May 18, 1988	31 min.	2300-2000 m
10	Aug. 31, 1988	2 hour 25 min.	2250-2100 m
11	Dec. 14, 1988	4 hour 31 min.	2100-2000 m
12	Jan. 18, 1990	47 min.	2500 m
13	April 18, 1990	6 hour 45 min.	1800 m
14	July 18, 1991	52 min.	2510-2400 m
15	Dec. 7, 1991		no eruption
16	Aug. 27, 1992	57 min.	2500-2100 m
17	Nov. 26, 1996		no eruption

Thus the second element of the model is the two separate paths to the eruption site, namely, the summit path and the rift zone path. Both 1 Hz and 2 Hz LP sources introduced as the first element are part of the rift zone path (see Figure 9 for a schematic view of the model).

As an example of how this model works, let us consider the rift zone eruption of December 14, 1988. LP events observed during the precursory crisis had a dominant frequency around 2 Hz. After 15 days of activity, the eruption suddenly stopped on December 29, 1988. We then observed, for a few days, a swarm of LP events with a dominant frequency of 1 Hz. This could be explained by our model in such a way that magma was supplied to the eruption site through the 2 Hz LP source, but the eruption stopped because the connection was made between the 1 Hz LP source and the eruption site, and the magma was drained back to the 1 Hz LP source from the eruption site. Such a drain back can explain the observation during the Puu Oo eruption at Kilauea, Hawaii, that the summit tremor has a maximum amplitude when the eruption stops at the end of each of many repeated episodes [*Koyanagi et al.*, 1988].

Another example is the seismic crisis on December 7, 1991, during which LP events were abundantly observed, as mentioned earlier. This episode may be considered as an intrusion into the rift zone without reaching the surface, a

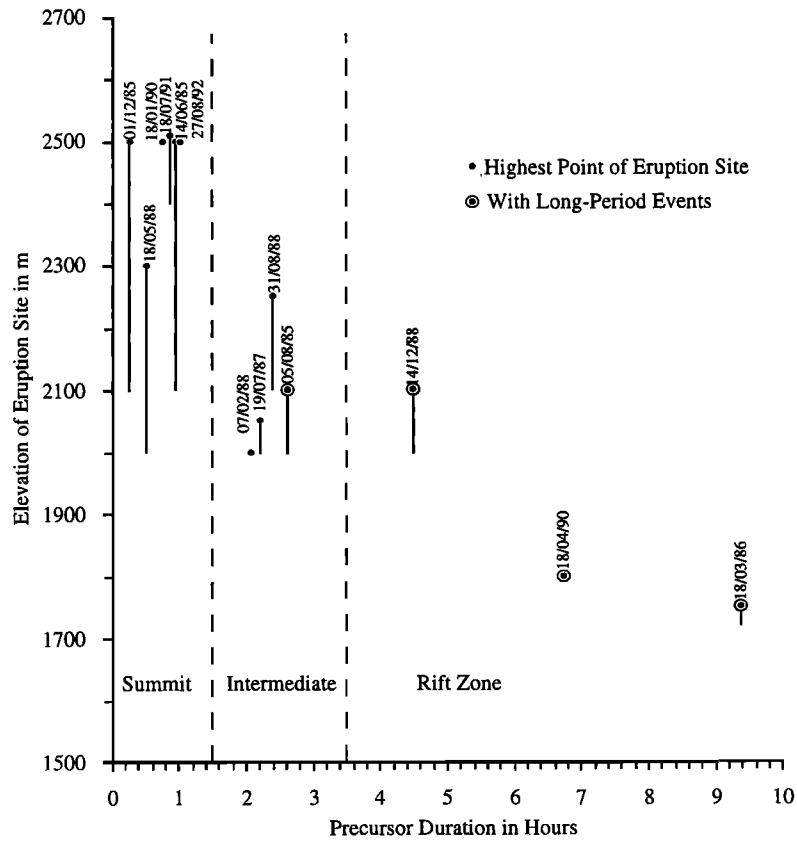

Figure 8. Relation between the precursor time of the seismic crisis and the elevation of the eruption site. Only those crises preceding the rift zone eruptions are accompanied by the occurrence of LP events.

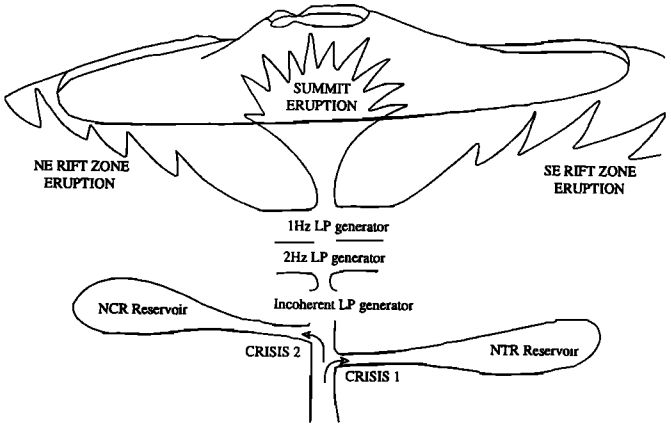

Figure 9. A schematic picture of the model drawn 4 days before the March 9, 1998, eruption. The actual depth was unknown at that time, but estimated later from hypocenter migration during the precursory crisis as described in section 5.

phenomenon commonly observed at Kilauea, Hawaii, where rift zones are well developed and accommodate magma intrusions.

Models for the magma system of the volcano have been proposed earlier by *Chevallier and Verwoerd* [1988] and *Lénat and Bachèlery* [1990]. *Chevallier and Verwoerd* [1988] distinguished a summit eruption from a rift zone eruption by attributing the former to hydrofracturing by magma in the column below the summit and the latter to the withdrawal of magma from the bottom portion of the magma chamber. On the other hand, *Lénat and Bachèlery* [1990] considered a large number of relatively small magma reservoirs filled from the depth during major oceanite eruptions like in 1977, and each of them became responsible for a smaller eruption until 1992. *Lénat and Bachèlery* [1990] emphasized the petrological and geochemical similarity of all the eruptions since 1977 rather than the difference between summit and rift zone eruptions.

Let us now proceed to the third element of our model, the magma reservoirs located deeper than the LP sources, to be introduced on the basis of observations on the spatial and temporal variation of coda localization.

4. Coda Localization

The data used for the study of coda localization are volcano-tectonic earthquakes with magnitude greater than about 2. As shown in Figure 7, the seismicity of shallow volcano-tectonic earthquakes beneath the summit declined since the eruption in August 1992 until 1996. However, a somewhat different trend was found for events with ***S-P*** times greater than 1 s. Both their frequency and maximum magnitude are low in 1993 and 1994, but increased significantly after the beginning of 1995. Their focal depths range from 10 to 30 km, and the largest one with M=2.5 occurred on March 2, 1996, at a depth of 15 km below sea level a few kilometers east of the central cone. It was followed by a cluster of seven events with M= 1.6 to 1.8 occurring at depths 16 to 18 km about 5 km northwest of the central cone in September 1996 and by an M=2.3 event under station CHR (now moved to nearby TCR) at a depth of 2 km below sea level. Then the first seismic crisis since the eruption of August 1992 occurred on November 26, 1996. This crisis consisted of 138 earthquakes located at about sea level beneath the central cone. The largest magnitude was 2.4, and the crisis lasted 104 min. We shall refer to this crisis as Crisis 1 to distinguish it from a minor crisis, which is referred to as Crisis 2 and consisted of 21 events with maximum magnitude 2.1, on August 23, 1997. After Crisis 2, the shallow seismicity beneath the summit maintained a high rate comparable to 1992 until the precursory crisis to the eruption on March 9, 1998.

4.1. Site Amplification Factor at the Network Stations

The coda method is based on the assumption that the spectral amplitude of coda waves can be expressed as a product of a factor which depends on the source only, a factor which depends on the recording site only, and a factor which is common to all sources and sites within a region. This assumption has been verified by observations in many parts of the world [e.g., *Sato and Fehler*, 1998].

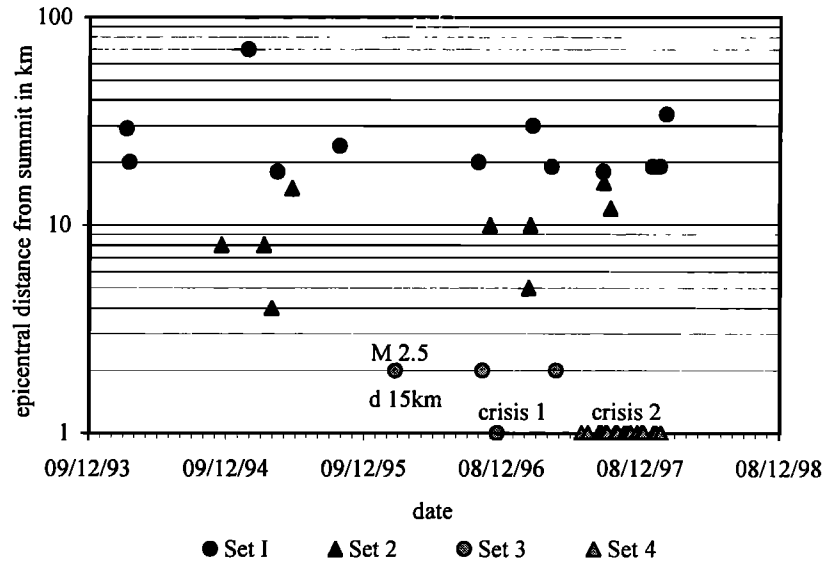

Figure 10. The distance from the summit to the epicenter of earthquake used for the coda analysis plotted against the time of occurrence of the earthquake. The data are divided into four sets in order to find the dependence of the coda localization on the distance and time.

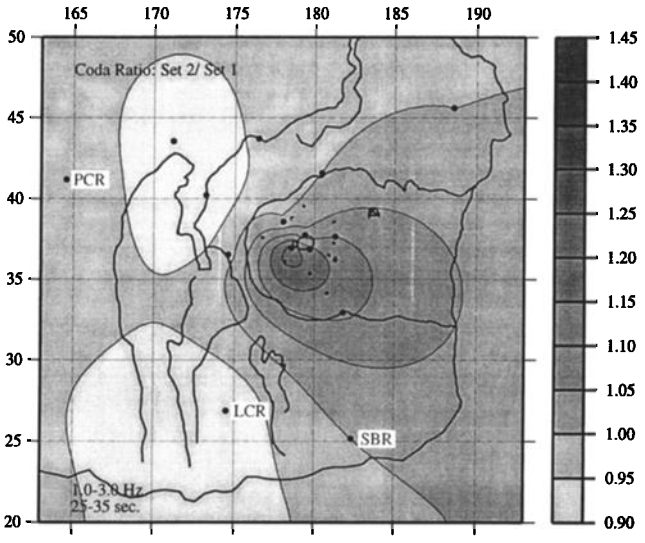

Figure 11. The ratio of the coda amplification factor for set 2 to that for set 1 as defined in Figure 10. Note that the contour interval is only 5%, demonstrating the precision of the map. See the caption of Figure 1 for the absolute location of the map.

However, the site amplification factor obtained for the stations of La Réunion systematically depends on the location of the source. The coda waves are strongly localized in the summit area when the source is under the summit. For example, the amplitude of coda in the summit area 30 s after the origin time can be 5 times larger than that at a station more than 15 km away.

In order to estimate the source effect on the coda amplification factor systematically, we applied the stochastic inversion method to data grouped according to the epicentral distance to the summit. Figure 10 shows the epicentral distance to the summit plotted against the time of occurrence for earthquakes used for the coda analysis. Two methods were used for calculating the coda amplitude. In the first one a band-pass filter is applied to the whole seismogram with the passband from 1 to 3 Hz, and the coda portion within a specified time window is printed. Two straight lines are drawn to leave half the peaks and half the troughs outside of them. The interval between the two lines at a given lapse time is measured as the amplitude. In the other method we compute the Fourier transform of the coda portion, integrate the squared amplitude in the frequency range from 1 to 3 Hz, and take its square root as the coda amplitude. In both methods we remove the effect of ambient noise obtained from the portion of record preceding the arrival of ***P*** waves assuming statistical independence between the signal and noise. The results from both methods are in good agreement.

The stochastic inversion method for coda amplification factor was first used by *Phillips and Aki* [1986] in order to avoid the use of a reference station and to deal with the data from stations which may not be in operation all the time. The recursive algorithm of *Zeng* [1991] vastly improved the method in computation efficiency, as demonstrated by *Su et al.* [1992]. This recursive inversion process was also called sequential estimation in the early literature [*Deutsch*, 1965; *Rodgers*, 1976; *Tarantola*, 1987], but *Zeng* [1991] was the first to show its power for analyzing seismological problems involving large, sparse matrices.

In order to find the source effect on the coda amplitude, the events were divided in two groups according to their epicentral distance from the summit, greater than 18 km in set 1 and ranging from 4 to 18 km in set 2, as shown in Figure 10. We applied the recursive inversion method to each set, and calculated the ratio of the amplification factor of set 2 to that of set 1. In Figure 11, the ratio normalized to PCR shows a smooth spatial variation contourable with an interval of only 5% and peaking at the summit area where the maximum value is 25% above PCR. From the above comparison, the source effect on the amplification factor determined from earthquakes of set 1 (listed in Table 4) may be considered less than 25% and may be neglected in comparison with the strong localization discussed in the following.

The numbers listed in Table 4 are very close to those used for the routine site effect correction of amplitude of various signals presented in section 3, and there is no need for revising any of the conclusions given there.

4.2. Coda Localization for Strong Sources Under the Summit

The first large event since the 1992 eruption was an M=2.5 event occurring, on March 2, 1996, a few kilometers east of the summit at a depth of 15 km below sea level, as shown in Figure 12. The second one is an M=2.4 event occurring during Crisis 1 on November 26, 1996, beneath the summit near sea level. The third one is an M=2.1 event occurring on July 25, 1997, about a month before Crisis 2. The fourth one is an M=2.1 event occurring during Crisis 2 on August 23, 1997. The last one is an M=2.4 event occurring on February 22, 1998, 2 weeks before the March 9, 1998 eruption. All these events except the first one occurred beneath the summit at about sea level.

Figures 12, 13a, 13b, 13c, and 13d based on the data given in Table 5, show the coda amplitude for the above five sources in the frequency band 1 to 3 Hz and the lapse time window 25 to 35 s corrected for the recording site effect using the amplification factor given in Table 4. The amplitude is normalized to station PCR located at about 15 km from the summit.

Figures 12 and 13 show that the distribution of coda amplitude is spatially smooth, as expected for diffusive waves, and each shows a localized region of peak amplitude. Except for the deep event, all shallow summit sources give peak amplitude about 5 times that of PCR (or TPR, which is located 27 km away from the summit). In all cases the amplitude decays to one half of peak value at about 5 km from the location of the peak. This represents a high concentration of scattered wave energy. If we

Table 4. Station Site Amplification Factor Determined From 14 Earthquakes With Epicentral Distance to the Summit Greater Than 18 km.

Station	Amplification Factor
BOR	1.0
DSR	0.41
SFR	0.84
TCR	0.74
NCR	0.93
NTR	0.86
PHR	0.61
PSR	0.27
PER	0.59
PBR	0.45
LCR	0.31
SBR	0.48
PCR	0.36
TPR	0.33
TXR	0.43
FLR	1.05

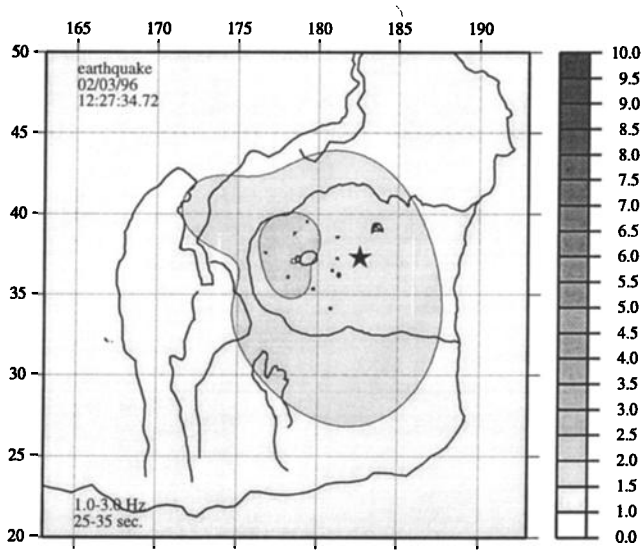

Figure 12. The coda amplification factor for the event 15 km deep east of the summit occurring at 1227 UT on March 2, 1996. The factor is normalized to station PCR, and the contour interval is 0.5. See the caption of Figure 1 for the absolute location of the map.

consider, as usual, that coda are composed of ***S*** waves with velocity around 3 km s^{-1}, the observed half decay distance of 5 km would lead us to conclude that the wavelength (about 1 km) is longer than the mean free path (a few hundred meters), putting the phenomenon into the regime of the Anderson localization [*Anderson*, 1958], which was predicted theoretically, but has never been observed in nature or the laboratory.

An alternative explanation is that the observed coda localization is due to very slow waves that can exist in the fluid-solid two-phase system The existence of waves slower than the acoustic waves in the fluid has been known for a fluid-filled crack [*Chouet*, 1986; *Ferrazzini and Aki*, 1987], lamination of fluid and solid [*Schoenberg*, 1984], and porous media [*Biot*, 1956]. For example, *Ferrazzini and Aki* [1987] showed that both the phase velocity and group velocity tend to zero as the wavelength increases to infinity for a fundamental symmetric mode in a fluid layer sandwiched between solid. Recently, *Yamamura* [1997] explained these slow waves by a common mechanism in which the pressure change in the fluid due to acoustic waves is relaxed by the coupled deformation in the solid. If the wave velocity is reduced by a certain factor, the wavelength will be shortened, and the mean free path will increase by the same factor, putting the coda localization into the diffusion regime. The consistency of the spatial-temporal

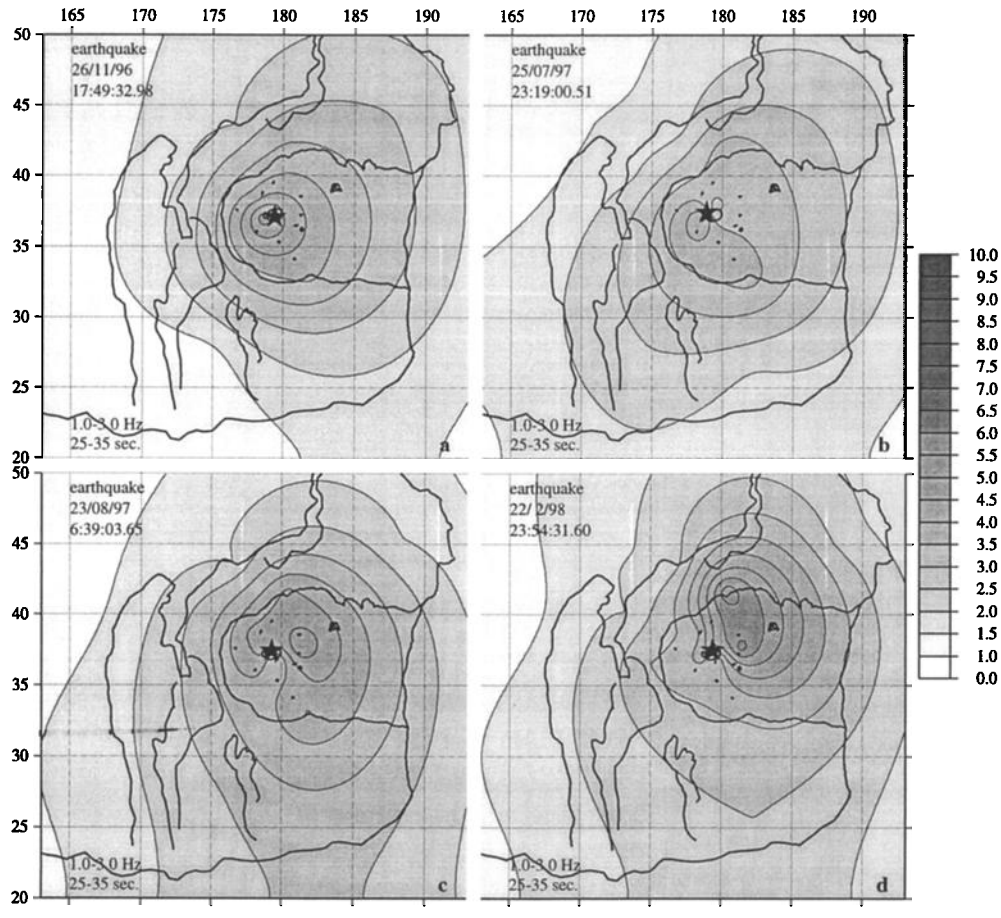

Figure 13. The coda amplification factor normalized to station PCR for large events occurring at about sea level beneath the summit at (a) 1749 UT on November 26, 1996, (b) 2319 UT on July 25, 1997, (c) 0639 UT on August 23, 1997, and (d) 2355 UT on February 22, 1998. See the caption of Figure 1 for the absolute location of the map.

Table 5. Amplitude of Coda at the Lapse Time of 30 s for the Frequency Band 1 to 3 Hz Normalized to PCR

station	March 2, 1996	Nov 26, 1996	July 25, 1997	Aug. 23, 1997	Feb. 22, 1998
BOR	2.38	5.88	5.90	4.00	3.66
DSR	1.74		3.71	3.80	2.86
SFR	2.19	5.59	3.53	5.00	4.21
TCR	2.21	4.59	3.65	4.48	3.11
NCR	1.64	4.12	4.24	5.00	5.20
NTR		4.59	4.94	4.48	3.33
PHR	1.21	3.29	3.35	3.08	2.90
PSR	1.14	2.59	2.82	2.36	2.45
PER	1.29	2.18	1.88	2.32	1.94
PBR	1.64	2.76	2.12	2.76	1.94
LCR	0.71	1.35	2.47	2.60	
SBR	1.19		2.47	2.60	2.31
PCR	1.00	1.00	1.00	1.00	1.00
TPR	1.07	1.24		1.08	1.07
TXR			1.94	1.96	1.94
FLR			4.65	6.56	5.02

pattern of the peak of coda localization with the magma process described below supports this explanation.

In addition to slow waves, Biot's theory predicts waves with higher velocity than the elastic velocity of the solid skeleton alone. These are attractive features as a model of magma body under the PdF, because seismic structure obtained by *Nercessian et al.* [1996] revealed a high velocity body under its summit.

4.3. Spatial-Temporal Pattern of Coda Localization and a Prediction of the Next Eruption

The peak region of coda localization found for the five strong sources made a systematic migration with time. The peak region for the earliest event lies NW of the summit, in agreement with the path of magma inferred from the locations of clusters of deep volcano-tectonic events in September 1996. The event during Crisis 1 shows the peak zone precisely in the summit area. Magma must have reached beneath the summit at this time, but instead of erupting to the summit, it moved SE (to station

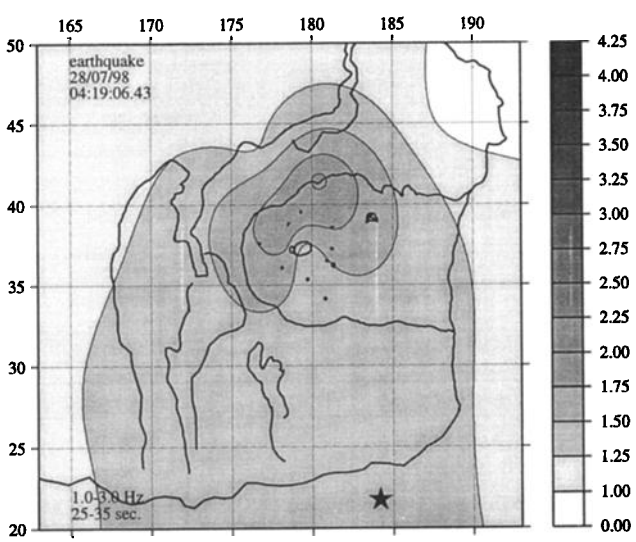

Figure 14. The coda amplification factor for the event at about sea level beneath the summit at 0704 UT on August 27, 1992, normalized to station PCR. See the caption of Figure 1 for the absolute location of the map.

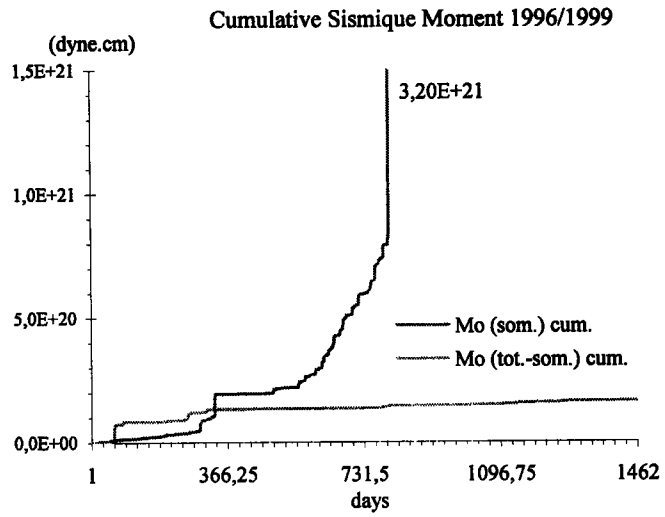

Figure 15. The cumulative seismic moment for the years 1996 through 1998. The curves for the events beneath the summit (marked as "som.") are shown separately from those outside the summit area (marked as "tot.-som.").

NTR), as indicated by the peak area of coda localization for the event occurring 1 month before Crisis 2. By the time of Crisis 2, magma stopped spreading SE, and at Crisis 2 it moved toward FLR and then NCR, as indicated by the peak areas for the event during Crisis 2 and the later one.

A question remains on the coda localization: why the peak region moves instead of expanding as the region filled with magma expands? A tentative answer to this puzzle would be the formation of a relatively hard shell surrounding the magma as it makes contact with the colder body of the volcano. The shell may be composed of harder material than the surrounding solid because of filling cracks existing in the body of volcano. The formation of hard shell may act adversely to the generation of slow waves according to the mechanism explained by *Yamamura* [1997].

It is interesting to note that there is a relatively flat area in the Enclos caldera seemingly bounded by the local caldera wall with a short radius of curvature near both NTR and NCR. The elevation is about 200 m higher near NCR than NTR. If these are the surface expression of magma reservoirs identified by *Bachèlery* [1981] as collapsed blocks, it is natural to put the NCR reservoir at a higher level than the NTR reservoir. Then it is also natural for the latter to be filled before the former by the ascending magma.

We compare the temporal-spatial pattern of coda localization with that observed at the time of the August 1992 eruption. There was a M=2.2 event during the seismic crisis preceding the eruption, but it was disturbed by a smaller event following it. So the coda amplitude could only be measured for the lapse time window 11 to 16 s. The result is shown in Figure 14, which is dominated by a high peak observed at NCR. In terms of the model depicted in Figure 9, this means that a summit eruption may occur when the NCR reservoir is filled completely. The NTR reservoir was filled during 9 months between Crisis 1 and Crisis 2. If the two reservoirs have a similar size, the filling of the NCR reservoir may take about the same time. We then expect a seismic crisis in May 1998 which will precede a summit eruption according to the model shown in Figure 9,

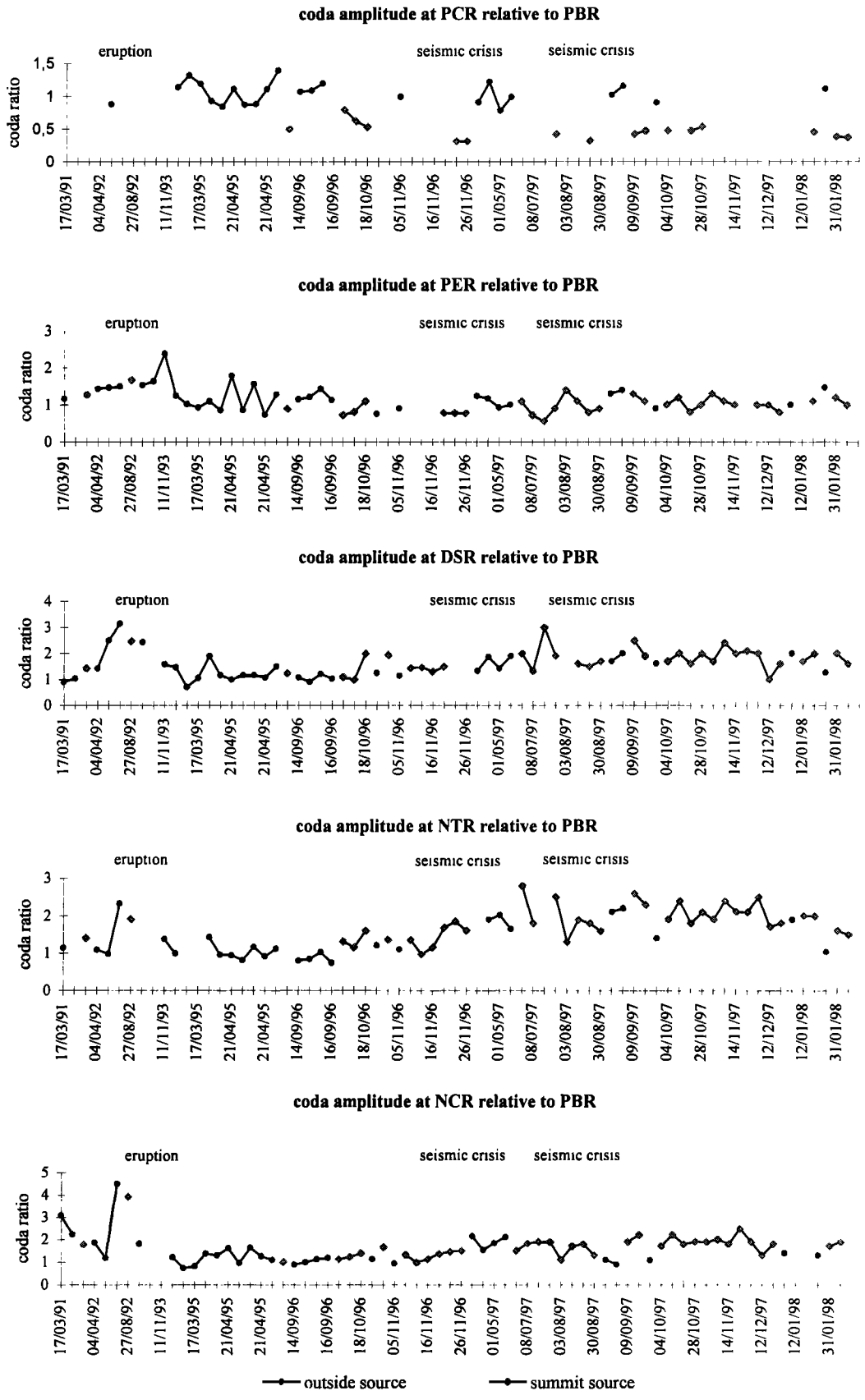

Figure 16. The coda amplitude at PCR, PER, DSR, NTR, and NCR relative to that at PBR plotted in the chronological order of events used for the measurement.

unless we observe LP events, in which case we should be prepared for a rift zone eruption.

This prediction of the May eruption was written on March 4, 1998, as a part of a manuscript for the observatory's Seismology Annual Report for 1997. It was based on the assumption that Crisis 2 marked the beginning of filling the NCR reservoir. The cumulative moment curve for the volcano-tectonic events shown in Figure 15, however, indicates that the high seismicity rate started about a month earlier than the time of Crisis 2. This revision would predict the March eruption more precisely.

4.4. Temporal Variation of Coda Amplitude at Selected Stations Relative to Station PBR

In order to examine the validity of the temporal-spatial pattern of coda localization obtained above from a small number of large events, we check the reality of temporal variation for selected stations using many events. At stations far away from the summit, the relative coda excitation should not show any significant temporal variation. In Figure 16 the coda amplitude at a station is plotted relative to PBR (about 7 km from the summit) as a function of the chronological event order, separately for events with an epicentral distance to the summit greater or smaller than 2 km. The coda amplitude at PCR (15 km from the summit) is presented in the first plot of Figure 16 and shows a strong difference between the summit source and distant sources. The amplitude ratio, however, is very stable in time for the same source type. Another example of stability is for station PER (nearly the same distance from the summit as PBR). Except for the possible aftereffect of the 1992 eruption, the coda ratio is constant, and shows no change from the time of the M=2.5 event on March 2, 1996, until the March 1998 eruption. On the other hand, all of the stations closer to the summit than PBR show significant increase in the coda amplitude relative to PBR after the time of the M=2.5 event. As examples, the ratios for DSR, NTR, and NCR are shown in the lower three plots of Figure 16. We can even recognize the change in trend at the time of Crisis 2. It is interesting to note that the difference between the summit source and those outside the summit area is not very strong for most of these stations. These plots leave no doubt about the reality of the temporal change in the distribution of coda amplitude.

In order to find more definitive support for the spatial pattern of the coda localization obtained from selected large events, we applied the recursive stochastic inversion method to a larger set of data systematically sampled in space and time.

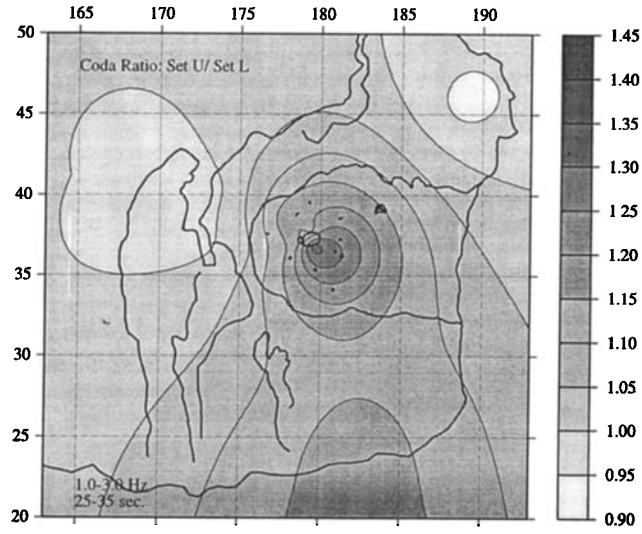

Figure 17. The ratio of the coda amplification factor for set U (after 1996) to that for set L (before 1996) avoiding the use of the near summit events. See text for a more precise definition of sets U and L. Note that the contour interval is only 5%, demonstrating the precision of the map. See the caption of Figure 1 for the absolute location of the map.

4.5. Testing the Spatial-Temporal Pattern of Coda Localization by Applying the Inversion Method to Systematically Grouped Data

Let us first confirm the increase of coda amplitude in the summit area during the 2-year period from early 1996 to March 1998 as compared to the preceding 2-year period. Since there were no events near the summit in the first 2-year period as shown in Figure 10, we delete all the events located horizontally within 3 km from the summit, and define set L as events before January 1996 and set U as those after. The inversion method described earlier for determining the site amplification factor is applied for each data set, and the ratio of the set U to the set L at

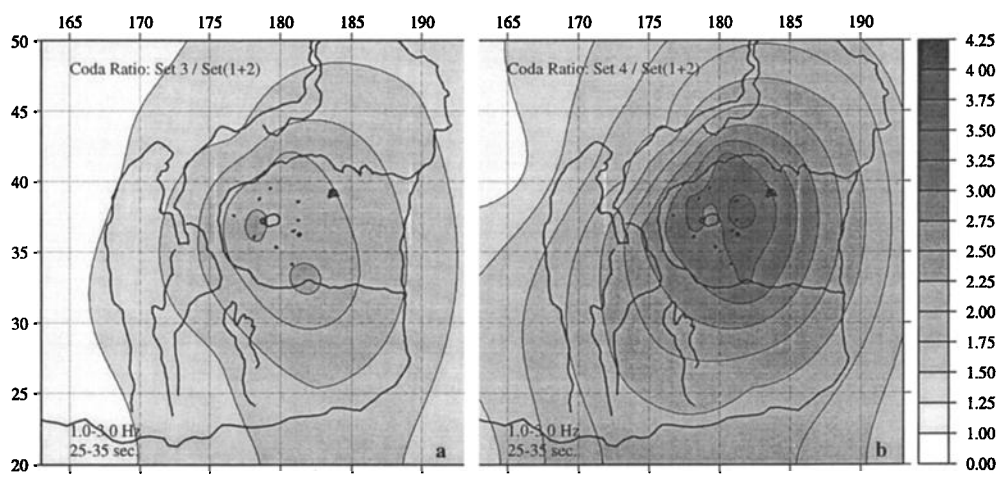

Figure 18. The ratio of the coda amplification factor for (a) set 3 to set 1 plus set 2 and (b) set 4 to set 1 plus set 2 as defined in Figure 10. The contour interval is 0.2. See the caption of Figure 1 for the absolute location of the map.

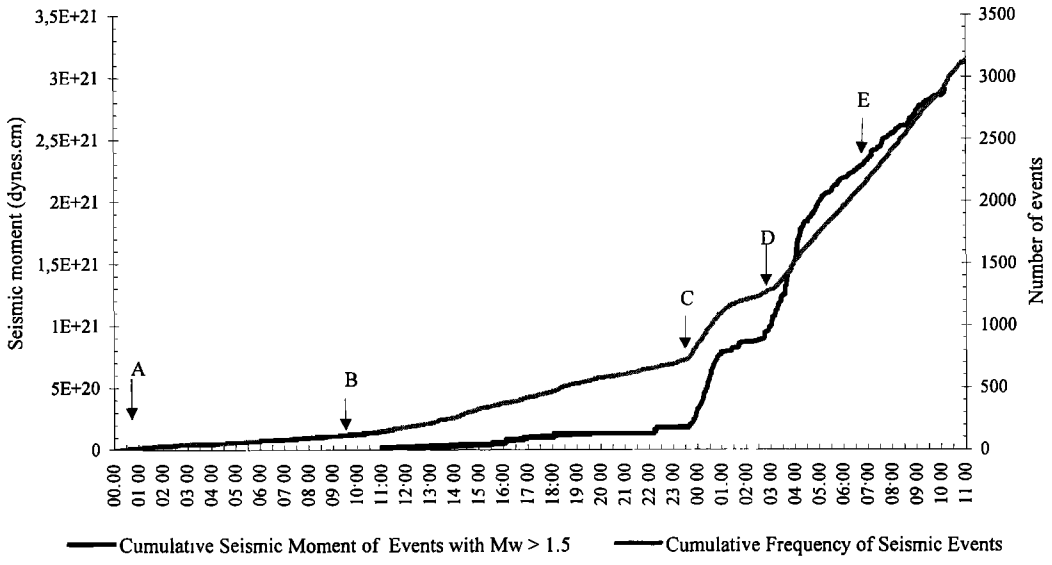

Figure 19. The cumulative seismic moment and number of volcano-tectonic events during the preeruption crisis of March 8 and 9, 1998. At A, focal depths of the events started at about 5 km below sea level; at B, they reached 3 km; at C, 2 km; and at D, 1 km. At E, the first 1 Hz LP event since 1993 appeared. The eruption started at 1105 UT on March 9, 1998.

each station normalized to PCR is plotted on a map and contoured as shown in Figure 17. Figure 17 shows a very smooth distribution centered at the summit where the ratio is a little over 30% above PCR. We had to delete two stations (NTR and LCR) in this contouring because of strong anomalies centered at each of them, probably due to long-term change in instrument calibration. The anomalies at LCR and NTR were 60% and 47% respectively, and they had to be discarded in this map, but we keep these two stations in other maps shown below where the range of amplitude variation is much greater across the network. From Figure 17, we may conclude that the increase in the coda localization since early 1996 is significant even for the sources outside the summit area, and is roughly concentric with the summit as the center.

Next, we grouped the earthquakes in the summit area during the period including Crisis 1 as marked set 3 in Figure 10. Applying the recursive inversion method to this group, and correcting the resultant amplitude for the station amplification factor given in Table 4, we plot the amplitude normalized to PCR in Figure 18a. The result shows a pattern of strong localization along the SE trending zone passing the southwestern side of the central cone supporting our earlier suggestion on the magma movement during this period.

Finally, we grouped 20 earthquakes occurring in the summit area after Crisis 2 as set 4 (Figure 10). The same analysis as above produced a map of coda localization as shown in Figure 18b. The peak region now moved to the northeastern side of the central cone, suggesting that the magma is moving toward NCR at this time.

4.6. Model Constructed Before the March 1998 Eruption

In section 3 we began to construct our model by distinguishing the summit path to eruption from the rift zone path, and introduced 1 Hz and 2 Hz LP sources as part of the rift zone path. In section 4 we introduced the NTR and NCR reservoirs located below these LP sources. A schematic view of the model is shown in Figure 9.

In Figure 9 we distinguish coherent and incoherent LP sources. The coherent source means that the waveforms are the same among the three summit stations, as in the example shown in Figure 3. All the LP events observed before September 1993 showed such coherence. After that we began to observe LP events which lost this coherence, and all the LP events after January 1994 showed incoherent waveforms among the summit stations. We place the source of incoherent LP events deeper than those of coherent ones, because they disappeared last.

The last LP event of the last active period confirmed to originate from beneath the summit area occurred on April 1, 1995. Its dominant frequency was 2.6 Hz, and the waveforms are incoherent among the three summit stations. The first LP event since then confirmed to originate from beneath the summit area occurred on June 4, 1997. The dominant frequency of this event was 2 Hz, and the waveforms are incoherent among the three summit stations. Thus the last disappearing is similar to the first reappearing, supporting the validity of the model depicted in Figure 9. The time of the appearance is near the end of the presumed filling of the NTR reservoir and the beginning of filling the NCR reservoir, suggesting the proximity of the incoherent 2 Hz LP source to these reservoirs.

The model may also explain why an eruption did not follow Crisis 1. At that time the LP event had not reappeared, and the coda localization was not as strong as that observed before the August 1992 eruption. The ascending magma had to fill the deep reservoirs before reaching the summit and rift zone path to the surface. The depths of these reservoirs will be estimated in section 5, from the hypocenters of volcano-tectonic events occurring immediately before the eruption.

The seismicity of volcano-tectonic earthquakes at all depths was extremely quiet for several months after Crisis 1 as shown in Figure 15. During this period, however, the coda localization was intensified and spread to the southwestern part of the

Enclos caldera. Either the magma transfer was smooth or the structure involved was detached from the source of volcano-tectonic earthquakes.

5. Testing the Model Through the Eruption From March 9 to September 21, 1998

Let us now describe how the model constructed in sections 3 and 4 functioned through the seismic crisis precursory to the eruption of March 9, 1998, and through the subsequent eruption period that lasted until September 21, 1998.

5.1. Precursory Seismic Crisis

As described in *Staudacher et al.* [1998], the precursory swarm of volcano-tectonic events started about 0000 UT on March 8, 1998, at a depth about 5 km below sea level beneath the central cone, and the depth of their hypocenters showed an unusually systematic upward migration at the average speed of about 3 km d^{-1}. The cumulative seismic moment curve shown in Figure 19 began a sharp rise at about 0000 UT on March 9 when the mean focal depth of the swarm reached about 2 km below sea level. The moment curve slowed down for a few hours when the mean focal depth was about 1 km below sea level before rising sharply again at 0300 UT. The first 1 Hz LP event since 1993 appeared at 0619 UT when the focal depth of the swarm reached sea level, about 5 hours before the eruption.

We can now infer depths of some elements of our model (Figure 9) from the above observation. Since the starting point of the precursory hypocenter migration must be the inlet to the NCR reservoir according to our model, the depths of NCR and NTR reservoirs and the sources of incoherent 2 Hz LP events are estimated to be around 5 km below sea level, which is within the volcanic edifice above the preexisting oceanic crust according to *Driad* [1997]. Likewise, the depth of the 1 Hz LP tremor is estimated to be just below sea level, supporting the estimate made in section 3.

The waveform of the first 1 Hz LP event, however, was not coherent among the three summit stations, unlike those presented in section 3. Our tentative explanation of this difference is that the coherent waveform may require a horizontally extended magma body, which may not have developed at this stage. This means that the structure of a magma system must evolve with time.

After the first 1 Hz LP event at 0619, there were no significant LP events until about 1020 when a continuous LP tremor appeared in the background of the swarm of volcano-tectonic events. The spectral shape of the tremor is similar to that of the first LP event. The amplitude distribution of the LP tremor is rather striking. It is peaked at the summit stations, but the attenuation with distance is very slow to certain directions, as shown in Figure 20, where the amplitude distribution of tremor in the frequency band 1.5 to 2.5 Hz around 1024 UT is shown. Such a slow decay was observed for some LP events discussed in section 3. This may be explained either by an extended source region of the tremor or by a waveguide effect due to an elongated magma body.

As described by *Staudacher et al.* [1998], the eruption started 1105 UT on March 9, 1998, from a 150 m long NS fissure at an elevation of 2450 m on the north flank of the central cone. The fissure system extended in an en echelon pattern to 2100 m elevation. Vigorous fountaining continued through the night of March 9. This pattern of eruption clearly indicates that the magma took the summit path defined in section 3.

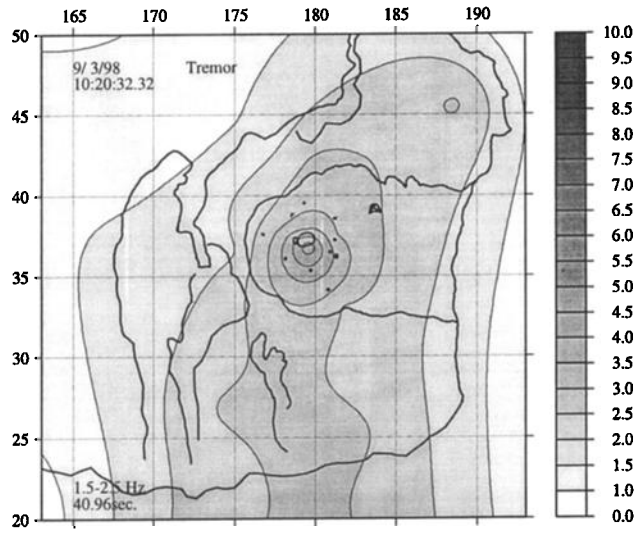

Figure 20. The amplitude distribution of the preeruption tremor in the frequency band 1.5 to 2.5 Hz obtained by the fasr Fourier transform (FFT) applied to the 40 s duration about 43 min before the eruption. See the caption of Figure 1 for the absolute location of the map.

This offered the first lesson we learned from this eruption about prediction. If we apply the empirical relation about the elevation of the eruption site, the presence of LP events, and the duration of precursory swarm, the eruption should have been through the rift zone path and the elevation of the eruption site should have been lower than 1800 m. Such a prediction overlooks a likely scenario in which the magma tries to go through the summit path and the rift zone path simultaneously. As soon as the magma overcomes the resistance in the summit path, the rift zone path is temporarily abandoned.

5.2. Seismic Tremors Originating From the Eruption

The eruption started with a lava flow from a fissure near the summit of the central cone, and extended downward in en echelon segments. The curtain of lava fountains was formed along the fissures, but the one along the summit slope disappeared in about 10 hours, and the eruptive activity became concentrated at two centers, named "Piton Kapor" and "Maurice and Katia Krafft" crater, as shown in Figure 21, at an altitude of 2150 m and 2080 m, respectively, in the intermediate range between the summit path and the rift zone path as classified in Figure 8.

Figure 22 shows the tremor amplitude observed at station PHR averaged over 10 s, plotted against the time of measurement. The amplitude can be safely considered as the intensity of the tremor source because of the stability of the propagation path effect on this relatively distant station (6 km from the Piton Kapor). At any time during the eruption episode, the isoamplitude contour at epicentral distances greater than 5 km became roughly circular with the center close to Piton Kapor and M. and K. Krafft craters. Typical examples are shown in Figures 23a and 23c, where the amplitude of tremor, corrected for the station site effect using Table 4, is mapped for frequency bands 0.5-1.5 Hz, and 1.5-2.5 Hz, respectively, at around 0527 UT on April 5, 1998. The decay of amplitude from the source shown in Figures 23a and 23c is similar to that of seismic waves

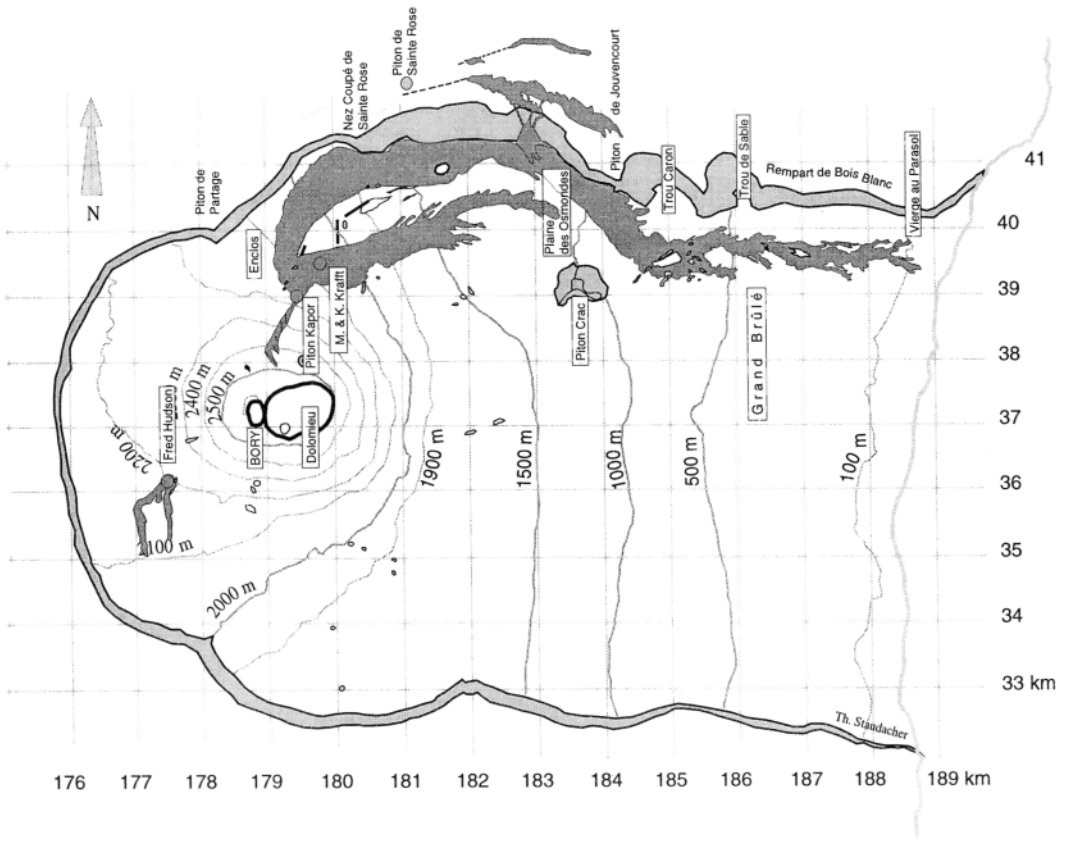

Figure 21. Three main vents of the March 1998 eruption are Piton Kapor, M. and K. Krafft, and F. Hudson. Eruption outside the Enclos caldera occurred in the last stage of the episode.

generated by rockfalls described in section 3. They fit well with the theoretical decay for surface waves with a Q factor of 40 to 60. The sharp decrease in amplitude across the summit caldera composed of low-velocity and high-attenuation material shown in Figures 23a and 23c also supports that they are surface waves. We also observed at TCR a phase difference of 90° between the vertical and horizontal component, corresponding to a retrograde motion for waves propagating from the east, suggesting that they correspond to the fundamental mode Rayleigh waves. An isolated eruption site named "Fred Hudson" southwest of the central cone opened on March 12 had a negligible effect on the tremor amplitude at any station.

The tremor amplitude shown in Figure 22 indicates a sharp rise and quick decay within about 10 hours after the beginning

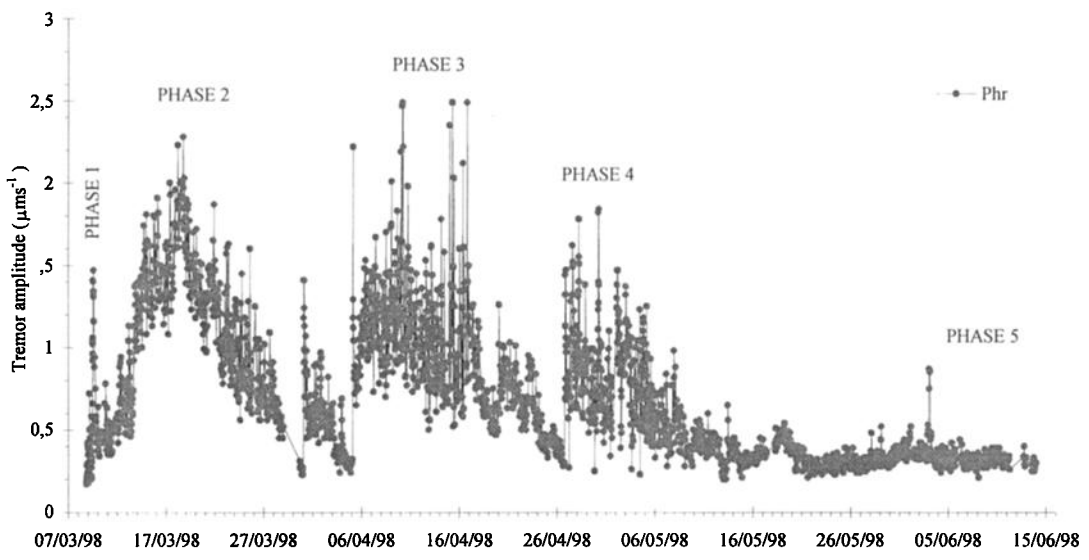

Figure 22. The amplitude of tremor at station PHR which is located at a distance of about 6 km WSW of the main eruption site. The amplitude is obtained by averaging the absolute value (in micrometers per second) over 10 s duration. See the caption of Figure 1 for the absolute location of the map.

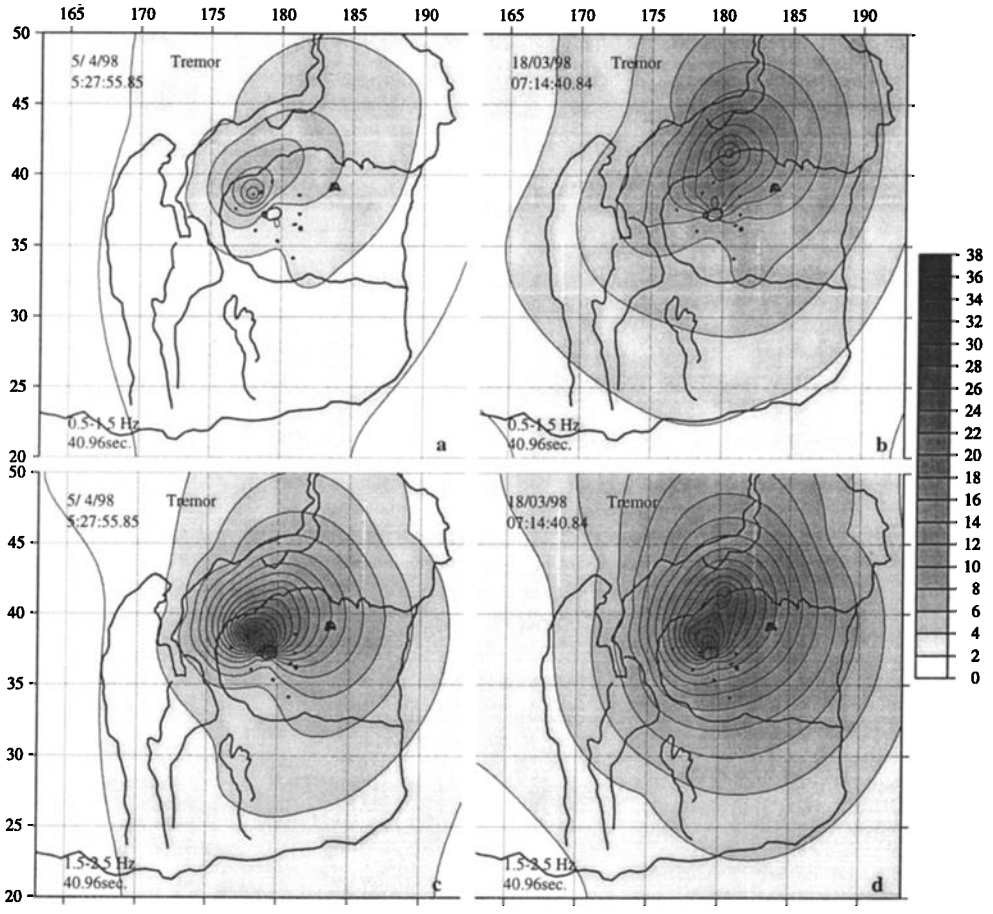

Figure 23. The amplitude distribution of tremor in the frequency band (a) 0.5 to 1.5 Hz and (b) 1.5 to 2.5 Hz obtained for the 40 s duration at 0527 UT on April 5, 1998, and in the frequency band (c) 0.5 to 1.5 Hz and (d) 1.5 to 2.5 obtained for the 40 s duration at 0714 UT on March 18, 1998. See the caption of Figure 1 for the absolute location of the map.

of the eruption. This corresponds to the vigorous fountaining from fissures opened successively downward starting from the one near the summit mentioned above. There are two steep rises in the tremor amplitude beginning on March 13 and 17, which do not appear to correspond to any changes in morphology of the eruption sites, except that the magma began to flow into lava tubes about this time. We interpret them as the opening connection to a magma reservoir through the rift zone path, because the zone of the maximum of the amplitude distribution during this phase extended to the summit area, as shown in Figures 23b and 23d, respectively, for the 0.5-1.5 Hz band and the 1.5-2.5 Hz band, suggesting magma movement through the rift zone path activating the LP tremor sources beneath the summit.

After about 2 months of strong variation, the tremor amplitude became nearly constant, implying a steady state flow of magma, with a constant pressure gradient through the conduit, or a constant excess pressure in the reservoir supplying magma to the eruption site. In order to maintain a constant pressure despite the withdrawal of magma, the reservoir must have a large capacity. This phase of the tremor amplitude history may be due to the opening of a direct connection between the eruption site and a large, deep reservoir.

5.3. The Last Phase of the Eruption Episode: Eruption Outside the Enclos Caldera

On July 28, an M=2.0 earthquake occurred at 0419 UT, offshore to the south of the summit, allowing the mapping of coda localization. Shown in Figure 24, for the frequency band 1 to 3 Hz, the peak zone is centered about the main eruption site, Piton Kapor, but is elongated in the northeast direction coincident with the rift zone in this area.

A swarm of LP events with peak amplitude near NCR on June 18 and 19 gave additional information about the condition of the magma system during the last phase of the eruption. An example of amplitude distribution is shown for the event recorded at 1257 UT on July 19 in Figure 25 for the frequency bands 0.5-1.5, 1.5-2.5, and 2.5-3.5 Hz. Their amplitude decay with distance is slower than for the tremor from Piton Kapor at short distances, indicating that their sources are deeper than the latter. The peak region of amplitude lies outside the Enclos caldera for the 0.5-1.5 Hz band, while it lies inside the caldera for the 2.5-3.5 Hz band. This may be due to the different frequency characteristics of waveguides developed in different parts of the volcano. Since the LP events are associated with the movement of magma, and the path of magma could be an

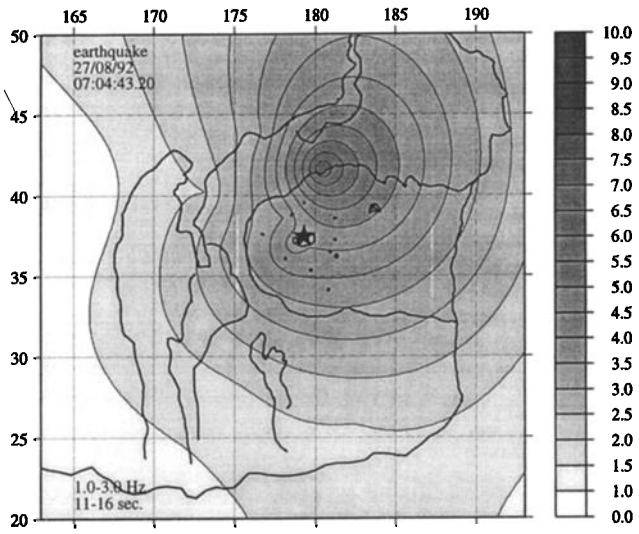

Figure 24. The coda amplification factor for the event located 16 km south of the summit at a depth of 23 km at 0419 UT on July 28, 1998, normalized to station PCR. See the caption of Figure 1 for the absolute location of the map.

efficient waveguide, it is reasonable to expect a strong wave guide effect on the amplitude of LP events. Thus the observed frequency-dependent amplitude distribution suggests that the waveguides (or magma paths) have been well developed not only inside, but also outside the Enclos caldera.

The tremor amplitude has been steady until the end of June, as shown in Figure 26, where the amplitude at station TCR is plotted instead of PHR because of decreasing signal-to-noise ratio as the eruption approaches the end. The amplitude shows a sudden increase on July 10, corresponding to a collapse of the Piton Kapor cone. It was followed by a period of strong variation in amplitude which lasted for about a week. After that a slow, smooth decrease lasted until August 6. The swarm of LP events near NCR, as well as the coda localization along the rift zone mentioned above, were observed during this period of decrease. This steady decrease suggested a decline of magma supply from the source, but the occurrence of a swarm of LP events and the elongated pattern of coda localization along the rift zone raised some concern about the eruption extending outside the Enclos caldera, which could become hazardous to population.

On August 6 and 7 a sharp rise in tremor amplitude was observed, followed by a period of large variation in amplitude. On August 9 an eruption outside the Enclos caldera started, confined in an area close to the caldera boundary as shown in Figure 21, and the amount of magma erupted was not large enough to cause any damage to population.

After mid-August the tremor amplitude again showed a slow, steady decrease with several minor upheavals each lasting 1 or 2 days, as shown in Figure 26. On September 21 the degassing from Piton Kapor was no longer visible, and the tremor amplitude decreased to the normal noise level.

6. Toward a Quantitative Modeling of an Eruption

In order to simulate the eruption episode quantitatively, we constructed a model composed of "reservoirs" connected to the source of magma at depth, to the eruption site at the surface, and to each other through "channels". This model is basically similar to electrical analog models proposed by *Decker* [1968, 1987] and *Shimozuru* [1981].

First, we describe the simplest case of a single reservoir which receives magma from below at a constant rate Q_0. When the

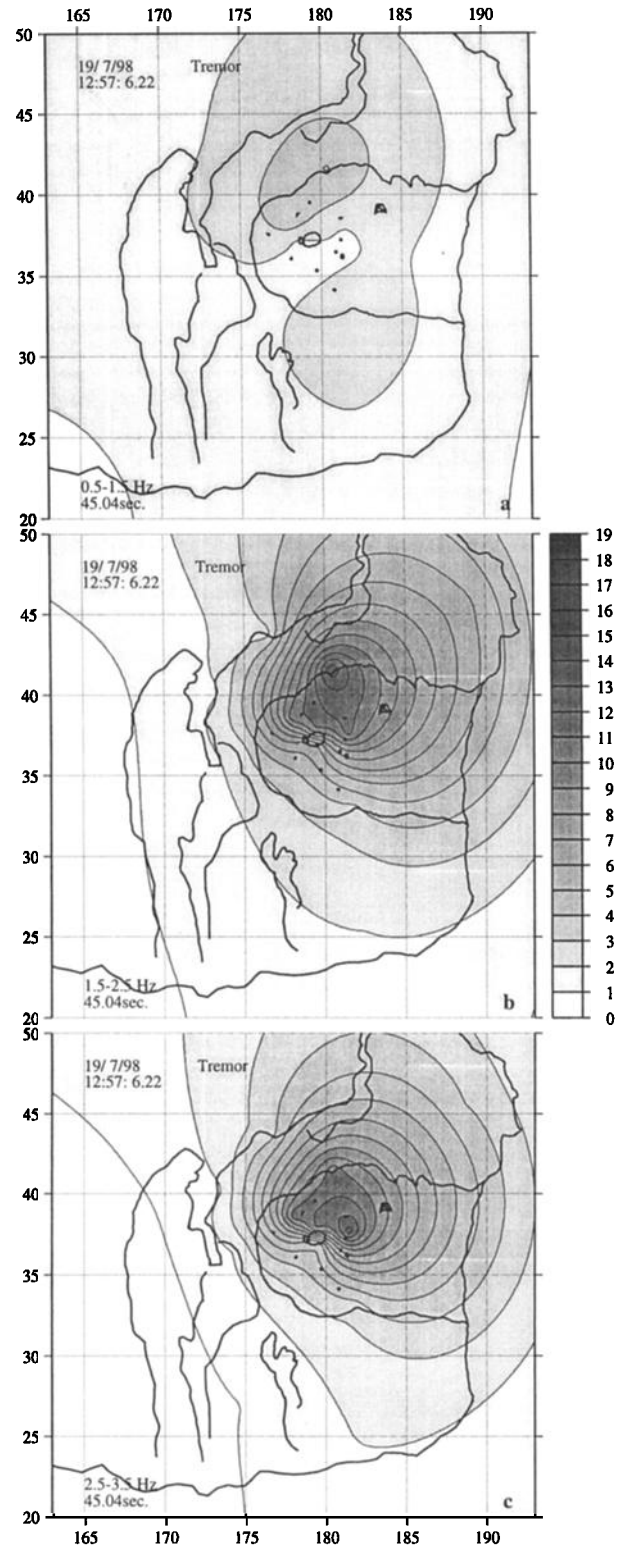

Figure 25. The amplitude distribution of an LP event in the frequency band (a) 0.5 to 1.5 Hz (b) 1.5 to 2.5 Hz, and (c) 2.5 to 3.5 Hz obtained by the FFT applied to the 18 s duration at 1257 UT on July 19, 1998. See the caption of Figure 1 for the absolute location of the map.

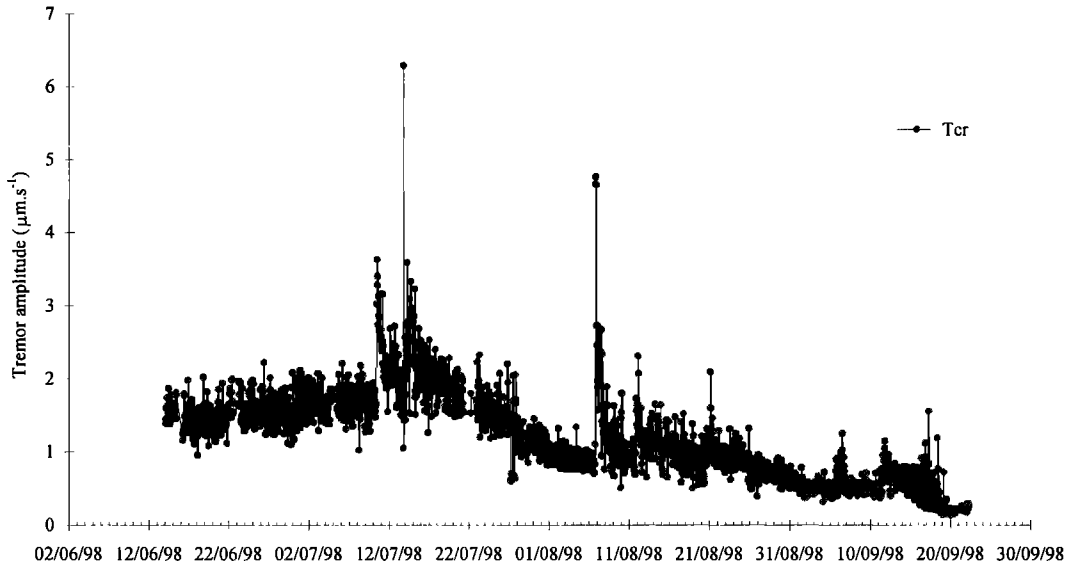

Figure 26. The amplitude of tremor at station TCR which is located at about 1.4 km WSW of Piton Kapor. The amplitude is obtained by averaging the absolute value (in micrometers per second) over 10 s duration.

excess pressure (pressure in excess of the hydrostatic pressure) in the reservoir reaches a critical value P_c, the channel to the surface opens and an eruption starts. The excess pressure P in the reservoir and the flow rate Q through the channel may be related by $P = RQ$, where R is the resistance of the channel. On the other hand, the rate of pressure increase in the reservoir may be related to the net inflow by the relation $dP/dt = (Q_0 - Q)/C$, where C is the capacity of the reservoir. For an episodic eruption, we need another parameter to stop the flow. We introduce the critical flow rate Q_c below which a channel closes or freezes. Q_c must be greater than Q_0 for an eruption to be episodic. Otherwise, the eruption becomes stationary at a flow rate of Q_0. This model is essentially static, neglecting the dynamic effects of magma flow and dike propagation, as well as the pressure change in the reservoir due to phase transition, chemical reaction, etc.

In a single-reservoir system, the flow rate starts with the value P_c/R and decreases nearly exponentially with the decay time constant RC. Such decays were observed repeatedly in the tremor amplitude history presented in Figures 22 and 26. The range of decay time shown in these figures is very broad, from several hours to more than a month, suggesting a broad range of the resistance of channels and capacitance of reservoirs under PdF.

The time interval of consecutive eruptions, on the other hand, is CP_c/Q_0, and the amount of magma in each eruption is CP_c. For example, the case of an eruption of 10 million m^3 once a year corresponds to Q_0 = 10 million m^3 y^{-1}, and the capacity C = 100,000 m^3 bar^{-1} if we take a critical excess pressure value of P_c = 100 bars.

In order to simulate the precursor-eruption phenomena observed during the March-September 1998 eruption episode, we consider a system composed of three reservoirs and five channels. The three reservoirs are (1) the upper reservoir within the volcanic edifice suggested from observations on LP events, (2) the lower reservoir suggested from observations on coda localization, and (3) the one below the preexisting oceanic crust. The system is sketched in Figure 27 together with the resultant reservoir pressures, channel flow rates and cumulative amount of magma plotted against time, assuming that all the excess pressure and the flow rates are zero at t =0. This initial condition may be oversimplified, but acceptable, because of the low seismicity of both volcano-tectonic and LP events as well as the weak coda concentration under the volcano around 1994. The channels 3, 4, and 5 shown in Figure 27 correspond to the summit path, rift zone path, and the path to outside the Enclos caldera, respectively. In addition to the critical excess pressure and capacity for each reservoir and the critical freezing flow rate for each channel, we needed a delay time parameter to introduce a delayed opening of the rift zone path and the outside caldera path. The 19 parameters are listed in Table 6. As shown in Figure 27, a rapid rise of magma from the deepest reservoir (Q_1) occurs twice before the eruption, which may correspond to the observed Crisis 1, and 2. The largest magma output is from the rift zone path, and the total magma erupted is about 60 million m^3 in agreement with a preliminary estimate from surface observations. The flow rate, on the other hand, is highest for the summit path, and the peak value is 50,000 m^3 h^{-1}, or 14 m^3 s^{-1}, which lies within the range of estimates made on the surface. The assumed flow rate from the upper mantle is 1500 m^3 h^{-1}, which is about 30% greater than the average rate of erupted magma for the period from 1930 to 1985.

A comparison of modeling results with monitoring results will allow adjustment of model parameters for prediction. The modeling offers an inference on what is happening under the volcano. The seismic monitoring offers information about the location of magma (through the coda localization), about slow magma movements (through the LP events), and about sudden magma movements (through the swarm of volcano-tectonic events).

7. Discussion and Conclusion

The empirical relation between the duration of the precursory seismic crisis and the elevation of the eruption site shown in Figure 8 was obtained from eruptions between 1985 and 1992. The departure of the March 1998 eruption from this relation may be attributed to a subtle change in the magma system beneath the summit area. The LP events occurring during the 1985-1992 period showed nearly the same waveform and arrival

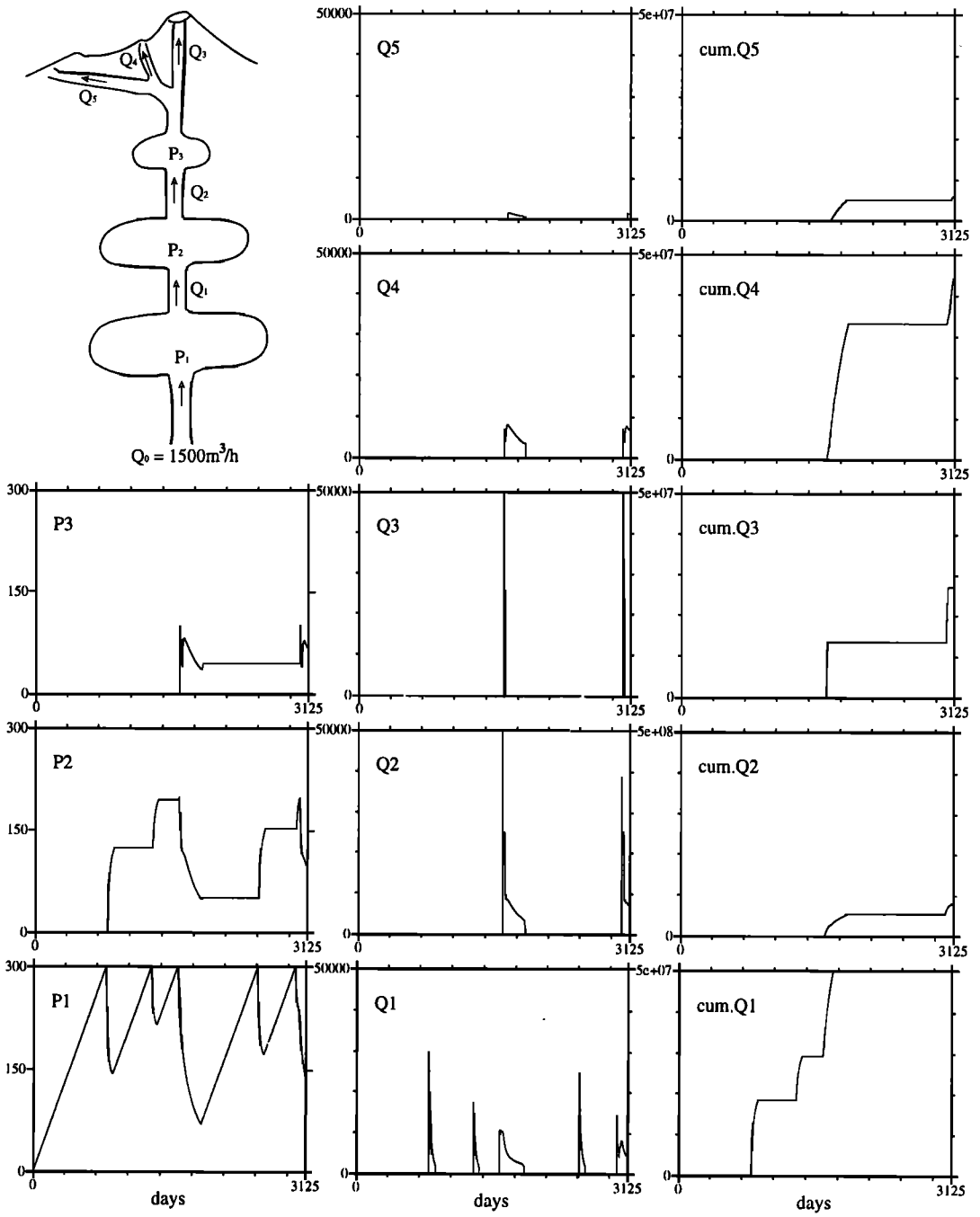

Figure 27. An example of the time plots of reservoir excess pressure P and channel flow rate Q for a three-reservoir and five channel system. A schematic view of the system is shown on the upper left. The parameters of the model are given in Table 6.

time at the three summit stations. On the other hand, the waveforms are different among these three stations for the LP events observed during the precursory period of the 1998 eruption, suggesting some difference in the location or structure of the source of LP events between the two periods. The mode of eruption was also different between the two periods. During the 1985-1992 period, moderate-sized eruptions (1 to 10 million m^3) occurred in a wide area rather uniformly through the summit and from both the northeast and the southeast rift zones. On the other hand, the 1998 eruption was concentrated on the north side of the summit. The source of LP events during the 1985-1992 period may be symmetric with respect to the summit center, while that during the 1998 eruption may be shifted toward the north.

The predictability of the eruption process will depend on how well we can constrain the model parameters using the monitoring data. Further work is needed to improve the quality of both the monitoring observation and the modeling. We may summarize in the following what we found about the volcano.

1. From 13 eruptions between 1985 and 1992, a strong correlation exists between the duration of the precursory swarm of volcano-tectonic events and the elevation of eruption sites,

Table 6. Model Parameters of the Three-Reservoir and Five-Channel System Shown in Figure 27

Parameters	Value
Flow rate from the upper mantle, m^3h^{-1}	1,500
Critical excess pressure, bars	
reservoir 1	300
reservoir 2	200
reservoir 3	100
Reservior capacity, m^3bar^{-1}	
reservoir 1	100,000
reservoir 2	150,000
reservoir 3	70,000
Channel resistance, bar $m^{-3}h^{-1}$	
channel 1	0.01
channel 2	0.004
channel 3	0.002
channel 4	0.01
channel 5	0.05
Freezing flow rate, m^3h^{-1}	
channel 1	2,000
channel 2	1,200
channel 3	20,000
channel 4	3,500
channel 5	750
Trigger delay time, hours	
channel 4 triggered by Channel 3	100
channel 5 triggered by Channel 4	1,000

precursor times being shorter than 1 hour for eruptions near the summit at 2500 m elevation, and longer than 6 hours for eruptions at elevations below 1800 m.

2. LP events are completely absent in the precursory crisis of summit eruptions, but they are present in all crises leading to flank eruptions occurring near the caldera rim. Combining this and the preceding item, we identify two separate paths to eruption sites, namely, the summit path and the rift zone path.

3. After the eruption of August 1992 (the last one before the 1998 eruption), we found the systematic disappearance of LP events dependent on the dominant frequency. LP events with dominant frequencies around 1 Hz disappeared first, while those with dominant frequencies around 2 Hz vanished last. Based on this observation, we infer that 1Hz LP sources are located above 2 Hz sources. This is confirmed by the earlier appearance of 2 Hz LP events than 1 Hz events during the precursory period for the 1998 eruption.

4. The coda site amplification factor systematically depends on the location of the seismic source, and shows a strong localization in the summit area when the source is beneath the summit. We attribute this localization of coda amplitude to slow waves trapped in the fluid-solid system.

5. The coda localization over the 2-year period preceding the 1998 eruption varied with time significantly. We attributed this change to the filling of reservoirs by the ascending magma, and predicted that the eruption will follow when the filling of reservoirs is completed.

6. The tremor originating from the eruption site was separated into five phases, each showing an approximately exponential decay. The decay time was the shortest (less than 1 day) in the first phase, and became longer for the later phases. The last phase showed a roughly constant amplitude for about 4 months. We attributed the time constant of amplitude decay to the product of the capacity of the reservoir and the resistance of the channel connecting the reservoir with the eruption site.

7. Finally, we attempted a computer simulation of the 1998 eruption using a model consisting of three reservoirs and five channels based on the above observations and interpretation.

Acknowledgments. We thank Bernard Chouet, Paul Delaney, Paul Davis, and an anonymous reviewer for their advice and criticism, upon which the original manuscript was extensively revised. We also thank Albert Tarantola and Jean Louis Cheminée for their leadership in making IPGP volcanological observatories places for research, and Patrick Bachèlery for helpful discussions on the geology of La Réunion. Patrick Bachèlery read an early version of the manuscript and gave us valuable advice for revision. We also thank the director of the Observatoire Volcanologique de la Piton de la Fournaise, Thomas Staudacher, the technical director, Philippe Kowalski, and all the members of the observatory for their conscientious and hard work in producing the excellent data on which the present work is based. This work was supported in part by the INSU under the PNRN 1995 project, CDP 95 31.08, and in part by the W.M. Keck Foundation.

References

Aki, K., Scattering conversions ***P*** to ***S*** versus ***S*** to ***P***, *Bull. Seismo. Soc. Am.*, *82*, 1969-1972, 1992.

Anderson, P. W., Absence of diffusion in certain random lattices, *Phys. Rev.*, *109*, 1492-1505, 1958.

Aster, R.C., G. Slad, J. Henton and M. Antolik, Differencial analysis of coda ***Q*** using similar microeartquakes in seismic gaps, I, Techniques and application to seismograms recorded in the Anza seismic gap, *Bull. Seismo. Soc. Am.*, *86*, 868-889, 1996.

Bachèlery, P., Le Piton de la Fournaise (Ile de La Réunion): Etude volcanologique structurale, these Univ. Clermont-Ferrand, Clermont-Ferrand, 1981.

Bachèlery, P., P.A. Blum, J.L. Cheminée, L. Chevallier, R. Gaulon, N. Girardin, C. Jaupart, X. Lalanne, J.L. LeMouel, J.C. Ruegg, and P.M. Vincent, Eruption at Piton de la Fournaise volcano on 3 February, 1981, *Nature*, *297*, 395-397, 1982.

Bachèlery, P., P. Kowalski, P. Catherine, J.C. Delmond, P.A. Blum, and J Croce, Precise temporal and mechanical identification of dike emplacement using deformation monitoring at Piton de la Fournaise, *2nd Workshop on European Laboratory Volcanoes, Santrini, Greece, 1996*, edited by R. Casale *et al.*, European Commission, pp. 475-485, 1998.

Biot, M.A., Theory of propagation of elastic waves in a fluid-saturated porous solid, I, Low frequency range, *J. Acoust. Soc. Am.*, *28*, 179-191, 1956.

Bonneville, A., J.-P. Barriot, and R. Bayer, Evidence from geoid data of a hotspot origin for the southern Mascarene plateau and Mascarene islands (Indian Ocean), *J. Geophys. Res.*, *93*, 4199-4212, 1988.

Briole, P., P. Bachèlery, B. McGuire, J Moss, J.C. Ruegg, and P. Sabourault, Deformation of Piton de la Fournaise: Evolution of the monitoring techniques and knowledge acquired in the last five years, in Proceedings, *2nd Workshop on European Laboratory Volcanoes, Santrini, Greece, 1996*, edited by R. Casale *et al.*, European Commission, pp. 467-474, 1998.

Chevallier, L., and W.J. Verwoerd, A numerical model for the mechanical behavior of intraplate volcanoes, *J. Geophys. Res.*, *93*, 4182-4198, 1988.

Chouet, B., Dynamics of a fluid driven crack in three dimensions by the finite difference method, *J. Geophys. Res.*, *91*, 13,967-13,992, 1986.

Chouet, B , Long-period volcano seismicity: Its source and use in eruption forecasting, *Nature*, *380*, 309-316, 1996.

Decker, R. W., Kilauea volcanic activity: An electrical analog model (abstract), *Eos Trans. AGU*, *49*, 352-353, 1968.

Decker, R. W., Dynamics of Hawaiian volcanoes: An overview, in Volcanism in Hawaii, edited by R.W. Decker, T.L. Wright, and P.H. Stauffer, *U. S. Geol. Surv. Prof. Pap.*, *1350*, 997-1018, 1987.

Delorme, H., P Bachèlery, P A. Blum, J.L. Cheminée, J.F. Delarue, J.C. Delmond, A. Hirn, J.C. Lépine, P.M. Vincent, and J. Zlotnicki, March 1986 eruptive episodes at Piton de la Fournaise volcano (Reunion Island), *J. Volcanol. Geotherm. Res.*, *36*, 199-208, 1989.

Deutsch, R., *Estimation Theory*, Prentice Hall, Englewood Cliffs, N. J., 1965.

Dieterich, J.H., Growth and persistence of Hawaiian rift zones, *J. Geophys. Res.*, *93*, 4258-4270, 1988.

Driad, L., Structure profonde de l'edifice volcanique de La Réunion (Ocean Indien) par sismique réfraction et grand angle, Ph.D. thesis, Univ. de Paris VII, Paris, 1997.

Dzurisin, D , R.Y. Koyanagi, and T.T. English, Magma supply and

storage at Kilauea volcano, Hawaii, 1956-1983, *J. Volcanol. Geotherm. Res.*, *21*, 177-206, 1984.

Fehler, M., P. Roberts and T. Fairbanks, ***Q*** temporal change in coda wave attenuation observed during an eruption of Mount St. Helens, *J. Geophys. Res.*, 93, 4367-4373, 1988.

Ferrazzini, V., and K. Aki, Slow waves trapped in a fluid-filled crack: Implication for volcanic tremor, *J. Geophys. Res.*, *92*, 9215-9223, 1987.

Grasso, J.R., and P Bachèlery, Hierarchical organization as a diagnostic approach to volcano mechanics: Validation on Piton de la Fournaise, *Geophys. Res. Lett.*, *22*, 2897-2900, 1995.

Hirn, A., J.C. Lépine, M. Sapin, and H. Delorme, Episodes of pit-crater collapse documented by seismology at Piton de la Fournaise, *J. Volcanol. Geotherm. Res.*, *47*, 89-104, 1991.

Hubbert, M.K., and W.W. Rubey, Mechanics of fluid filled porous solids and its application to overthrust faulting, *Geol. Soc. Am. Bull.*, *70*, 115-166, 1959.

Kato, K., K. Aki, and M. Takemura, Site amplification from coda waves: Validation and application to ***S*** wave site response, *Bull. Seismo. Soc. Am.*, *85*, 467-477, 1995.

Koyanagi, R Y., B. Chouet, and K. Aki, Origin of volcanic tremor in Hawaii, 2, Data from the Hawaiian Volcano Observatory 1969-1985, in Volcanism in Hawaii, edited by R.W. Decker, T.L. Wright, and P. H Stauffer, *U. S. Geol. Surv. Prof. Pap.*, *1350*, 1221-1258, 1987.

Koyanagi, R Y., W. R. Tanigawa, and J. S. Nakata, Seismicity associated with the eruption, in The Puu Oo Eruption of Kilauea Volcano, Hawaii: Episode 1 Through 20, January 3, 1983 Through June 8, 1984, edited by E.W. Wolfe, *U. S. Geol. Surv. Prof. Pap.*, *1463*, 183-236, 1988.

Koyanagi, S., K. Aki, N. Biswas, and K. Mayeda, Inferred attenuation from site-effect-corrected T phase recorded on the Island of Hawaii, *Pure Appl. Geophys.*, *144*, 1-16, 1995.

Lénat, J.-F , and P. Bachèlery, Dynamics of magma transfers at Piton de la Fournaise volcano (Réunion Island, Indian Ocean), in *Modeling of Volcanic Processes* edited by C.-Y. King and R. Scarpa, pp. 57-72, Fried. Vieweg, und Sohn, Brunswick, Germany, 1988.

Lénat, J.-F.,and P. Bachèlery, Structure et fonctionnement de la zone centrale du Piton de la Fournaise, in *Le Volcanisme de La Réunion - Monographie* edited by J.F. Lénat, pp. 257-296, Cent. de Rech. Volcanol., Obs. de Phys. du Globe de Clermont-Ferrand, Univ. Blaise Pascal, Clermont-Ferrand, 1990.

Lénat, J -F , P Vincent, and P. Bachèlery, The off-shore continuation of an active basaltic volcano: Piton de la Fournaise (Réunion Island, Indian Ocean), structural and geomorphologic interpretation from sea beam mapping, *J. Volcanol. Geotherm. Res.*, *36*, 1-36, 1989a.

Lénat, J.-F , P. Bachèlery, A. Bonneville, P. Tarits, J.L. Cheminée, and H. Delorme, The December 4, 1983 to February 18, 1984 eruption of Piton de la Fournaise (La Réunion, Indian Ocean): Description and interpretation, *J. Volcanol. Geotherm. Res.*, *36*, 87-112, 1989b.

Lénat, J.-F , P Bachèlery, A. Bonneville, and A. Hirn, The beginning of the 1985-1987 eruptive cycle at Piton de la Fournaise (La Réunion); new insights in the magmatic and volcano-tectonic systems, *J. Volcanol. Geotherm. Res.*, *36*, 209-232, 1989c.

Lépine, J.C , Répartition de la sismicité dans la zone d'extension de Djibouti 1972-1986. Relations entre activité sismique et éruptions volcaniques au Piton de la Fournaise, Réunion, 1985-1986, Ph.D. thesis, Univ. de Paris VII, Paris, 1987.

Londono, B.J.M., A.J.J. Sanchez, E.L.E. Tore, F.G. Cruz, and O.P. Bohorquez, Coda ***Q*** before and after the eruptions of 13 November 1985, and 1 September 1989, at Nevado del Ruiz volcano, Columbia, *Bull. Volcanol.*, *59*, 556-561, 1998.

Nakamura, K., Why do long rift zones develop in Hawaiian volcanoes-A possible role of thick oceanic sediments, *Bull. Volcanol. Soc. Jpn., Ser 2*, *25*, 255-270, 1980.

Nercessian, A., A. Hirn, J.C. Lépine, and M. Sapin, Internal structure of Piton de la Fournaise volcano from seismic wave propagation and earthquake distribution, *J. Volcanol. Geotherm. Res.*, *70*, 123-144, 1996.

Phillips, W.S., and K. Aki, Site amplification of coda waves from local earthquakes in central California, *Bull. Seismo. Soc. Am.*, *76*, 627-648, 1986.

Rancon, J.P., P. Lerebour, and T. Auge, The Grand Brule exploration drilling. New data on the deep framework of the Piton de la Fournaise volcano, 1, Lithostratigrapic units and volcanostructural implications, *J Volcanol. Geotherm. Res.*, *36*, 113-128, 1989

Rautian, T G., and V.I. Khalturin, The use of coda for determination of the earthquake source spectrum, *Bull. Seismo. Soc. Am.*, *68*, 923-948, 1978.

Rodgers, C. D., Retrieval of atmospheric temperature and composition from remote measurements of thermal radiation, *Rev. Geophys.*, *14*, 609-624, 1976.

Rousset, D., A. Lesquer, A. Bonneville, and J.-F. Lénat, Complete gravity study of Piton de la Fournaise volcano, Réunion Island, *J. Volcanol. Geotherm. Res.*, *36*, 37-52, 1989.

Sapin, M, A. Hirn, J.C. Lépine, and A. Nercessian, Failure and fluid flow from earthquakes of eruptions at Piton de la Fournaise volcano, *J. Volcanol. Geotherm. Res.*, *70*, 145-168, 1996.

Sato, H. and, M. Fehler, *Seismic Wave Propagation and Scattering in the Heterogeneous Earth*, 308 pp., Springer-Verlag, New York, 1998.

Schoenberg, M., Wave propagation in alternating solid and fluid layers, *Wave Motion*, *6*, 303-320, 1984.

Shimozuru, D., Magma reservoir systems inferred from tilt patterns, *Bull. Volcanol.*, *44*, 499-504, 1981.

Staudacher, T., P. Bachèlery, M. P. Semet, and J. L. Cheminée, Piton de la Fournaise, *Bull. Global Volcanism Network Smithson. Inst.*, *23* (3), 2-4, 1998.

Su, F , K. Aki, T L. Teng, Y Zeng, S. Koyanagi, and K. Mayeda, The relation between site amplification factor and surficial geology in central California, *Bull. Seismo Soc. Am.*, *82*, 580-602, 1992.

Tarantola, A., *Inverse Problem Theory: Methods for Data Fitting and Model Parameter Estimation*, Elsevier Sci., New York, 1987.

Thurber, C H , and A.E. Gripp, Flexure and seismicity beneath the south flank of Kilauea volcano and tectonic implications, *J. Geophys. Res.*, *93*, 4271-4278, 1988.

Walcott, R.I., Flexure of the lithosphere at Hawaii, *Tectonophysics*, *9*, 435-446, 1970.

Yamamura, K., Slow waves in the fluid-solid 2 phase system (in Japanese), M.S. thesis, Univ. of Tokyo, Tokyo, 1997.

Zeng, Y., Deterministic and stochastic modeling of the high frequency seismic wave generation and propagation in the lithosphere, Ph.D. thesis, Univ of South. Calif., Los Angeles, 1991.

Zeng, Y , Theory of scattered ***P*** and ***S*** wave energy in a random isotropic scattering medium, *Bull. Seismo. Soc. Am.*, *83*, 1264-1276, 1993

K. Aki and V. Ferrazzini, Observatoire Volcanologique du Piton de la Fournaise, 14 Route Nationale 3, 97418 La Plaine des Cafres, La Réunion, France. (aki@iremia univ-reunion.fr)

(Received November 5, 1998; revised January 3, 2000; accepted January 27, 2000)